




NSun2 regulates aneurysm formation by promoting autotaxin expression and T cell recruitment

Yutong Miao¹ · Yang Zhao² · Lulu Han¹ · Xiaolong Ma¹ · Jiacheng Deng³ · Juan Yang¹ · Silin Lü⁴ · Fangyu Shao¹ · Wei Kong¹ · Wengong Wang⁵ · Qingbo Xu³ · Xian Wang¹ · Juan Feng¹ 

Received: 22 February 2020 / Revised: 9 July 2020 / Accepted: 22 July 2020 / Published online: 30 July 2020
© Springer Nature Switzerland AG 2020

Abstract

Abdominal aortic aneurysm (AAA) is characterized by inflammatory cell infiltration and aggravated by hyperhomocysteinemia (HHcy). It is unknown whether the homocysteine (Hcy)-activated RNA methyltransferase NOP2/Sun domain family member 2 (NSun2) is associated with AAA. Here, we found that NSun2 deficiency significantly attenuated elastase-induced and HHcy-aggravated murine AAA with decreased T cell infiltration in the vessel walls. T cell labeling and adoptive transfer experiments confirmed that NSun2 deficiency inhibited the chemotaxis of vessels to T cells. RNA sequencing of endothelial cells showed that Hcy induced the accumulation of various metabolic enzymes of the phospholipid PC-LPC-LPA metabolic pathway, especially autotaxin (ATX). In the elastase-induced mouse model of AAA, ATX was specifically expressed in the endothelium and the plasma ATX concentration was upregulated and even higher in the HHcy group, which were decreased dramatically by NSun2 knockdown. In vitro Transwell experiments showed that ATX dose-dependently promoted T cell migration. HHcy may upregulate endothelial ATX expression and secretion and in turn recruit T cells into the vessel walls to induce vascular inflammation and consequently accelerate the pathogenesis of AAA. Mechanistically, secreted ATX interacted with T cells by binding to integrin $\alpha 4$, which subsequently activated downstream FAK/Src-RhoA signaling pathways and then induced T cell chemokinesis and adhesion. ATX overexpression in the vessel walls reversed the inhibited development of AAA in the NSun2-deficient mice. Therefore, NSun2 mediates the development of HHcy-aggravated AAA primarily by increasing endothelial ATX expression, secretion and T cell migration, which is a novel mechanism for HHcy-aggravated vascular inflammation and pathogenesis of AAA.

Keywords NSun2 · Abdominal aortic aneurysm · ATX · Endothelial cells · T cells

Abbreviations

AAA	Abdominal aortic aneurysm
ATX	Autotaxin
BrdU	5-Bromo-2'-deoxyuridine
CFSE	Carboxy fluorescein diacetate succinimidyl ester
FAK	Focal adhesion kinase

Yutong Miao and Yang Zhao contributed equally to this article.

Electronic supplementary material The online version of this article (<https://doi.org/10.1007/s00018-020-03607-7>) contains supplementary material, which is available to authorized users.

✉ Xian Wang
xwang@bjmu.edu.cn

✉ Juan Feng
juanfeng@bjmu.edu.cn

¹ Department of Physiology and Pathophysiology, School of Basic Medical Sciences, Peking University, Key Laboratory of Molecular Cardiovascular Science, Ministry of Education, Beijing 100191, People's Republic of China

² Department of Laboratory Medicine, Peking University Third Hospital, Beijing, People's Republic of China

³ Cardiovascular Division, BHF Center for Vascular Regeneration, King's College London, London, UK

⁴ State Key Laboratory of Bioactive Substances and Function of Natural Medicine, Institute of Materia Medica, Peking Union Medical College, Chinese Academy of Medical Sciences, Beijing, People's Republic of China

⁵ Department of Biochemistry and Molecular Biology, School of Basic Medical Sciences, Peking University, Beijing, People's Republic of China

Hcy	Homocysteine
HHcy	Hyperhomocysteinemia
HUVECs	Human umbilical vein endothelial cells
ICAM	Intercellular adhesion molecule
LPA	Lysophosphatidic acid
LPC	Lysophosphatidylcholine
NSun2	NOP2/Sun domain family, member 2
RhoA	Ras homolog gene family, member A

Introduction

Abdominal aortic aneurysm (AAA) is a typical asymptomatic disease leading to aneurysm expansion and rupture. The pathogenesis of AAA includes vascular inflammation, smooth muscle cell apoptosis, extracellular matrix degradation, and oxidative stress [1]. Despite progress in invasive surgical repair and drug treatment, the fatality rate is extremely high in patients once the aneurysm ruptures. Thus, it is of high importance to enhance our understanding of the pathobiology of AAA and develop new strategies to prevent the progression of AAA.

In AAA, multiple inflammatory cells, including neutrophils, T cells, B cells, macrophages, mast cells and NK cells, were observed in all layers of the aortic wall [2]. The processes of leukocyte recruitment to the aortic wall include selectin-dependent cell rolling, chemokine-induced cell activation, integrin-dependent cell adhesion and cell transmigration [3]. NSun2 (NOP2/Sun domain family, member 2; Myc-induced SUN domain-containing protein, Misu) is a nucleolar RNA methyltransferase implicated in cell proliferation [4], stem cell differentiation [5], testis differentiation [6], and human cancers [4, 7]. Our previous study reported that NSun2 upregulates the protein expression of intercellular adhesion molecule 1 (ICAM-1) by methylating ICAM-1 mRNA in vascular endothelial cells, thereby increasing the adhesion of leukocytes to the endothelium and promoting arteriosclerosis in rats [8]. However, whether NSun2 mediates murine AAA formation by affecting various inflammatory cell migration or adhesion is unclear, and if it does mediate AAA formation, the underlying mechanism is unknown.

Hcy is a sulfur-containing amino acid and serves as an intermediate product during the metabolism of methionine and cysteine. Hyperhomocysteinemia (HHcy), defined as a pathological elevation of plasma Hcy levels ($> 15 \mu\text{M}$) resulting from a metabolic imbalance, is an independent risk factor for various vascular diseases, including aneurysm [9, 10]. Our previous studies showed that HHcy accelerates AAA development accompanied by many more monocytes/macrophages and T cells in adventitia and activation of macrophage NLRP3 inflammasome [10, 11]. Hcy directly interacts with and activates the angiotensin II

type I receptor to aggravate vascular injury and AAA formation [12]. Recently, B cell-derived pathogenic anti- β 2-glycoprotein I (anti- β 2GPI) IgG and antiphospholipid (aPL) antibodies might contribute to HHcy-aggravated chronic vascular inflammation and AAA formation [9]. Although HHcy activates endothelial NSun2 methyltransferase activity to recruit leukocytes in arteriosclerosis [8], the potential regulatory targets of NSun2 in HHcy-accelerated murine AAA need to be further investigated.

Modification of cell membranes is detected in various vascular diseases, such as atherosclerosis and AAA. The presence of lipid-protein interactions in the membrane provides a substrate for lysophosphatidylcholine (LPC) and lysophosphatidic acid (LPA) [13]. Autotaxin (ATX; also known as ENPP2), a lysophospholipase D (lysoPLD) relying on its catalytic phosphodiesterase (PDE) domain, catalyzes the conversion of LPC to LPA [14]. LPA plays a critical role in lymphocyte migration and several kinds of tumor cell motility [14–17]. Although most research to date has focused on targeting the ATX-LPAR axis to treat patients suffering from various inflammatory diseases, emerging data point to the important role of ATX directly interacting with integrin on the target cell surface to regulate cell function as a secreted protein, lysoPLD. Here, the significance of ATX-mediated intercellular interactions in AAA is explored.

Using elastase-induced and HHcy-accelerated AAA models in NSun2^{+/-} mice, we demonstrated that the RNA methyltransferase NSun2 mediated HHcy-induced ATX expression and secretion from the endothelium, which in turn recruited T cells by binding to their integrin α 4 and subsequently aggravated AAA development in mice. Targeting ATX may be a potential novel target to treat HHcy-associated vascular inflammation and AAA.

Materials and methods

Reagents and antibodies

DL-Homocysteine, elastase from porcine pancreas and MnCl_2 were obtained from Sigma Chemical Co. (St. Louis, MO, USA). CFSE and BrdU were purchased from Invitrogen Corporation (Waltham, MA, USA). Recombined ATX was purchased from R&D Systems, Inc. (Minneapolis, MN, USA). Recombined CXCL12 was purchased from Novoprotein Scientific Inc. (Shanghai, China). HA130 was purchased from MCE (Monmouth Junction, NJ, USA). CD3 ϵ F(ab')₂ fragments and IgG isotypes were purchased from Bio X Cell (West Lebanon, NH, USA). Antibodies against CD3 ϵ , CD19, integrin α 4, p-FAK (Tyr397), FAK, p-Src (Tyr416) and Src were purchased from Cell Signaling Technology (Danvers, MA, USA). Antibodies against CD31 and β -actin and recombinant human ICAM-1 were

purchased from ABclonal (Wuhan, China). Antibodies against α -SMA and NSun2 and mounting medium with DAPI were purchased from Abcam (Cambridge, MA, USA). Antibodies against ATX were purchased from Santa Cruz Biotechnology (Dallas, TX, USA). Antibodies against RhoA were purchased from Cytoskeleton (Denver, CO, USA). Neutralizing antibody anti-CD49d mAb was purchased from BD Biosciences (Franklin Lakes, NJ, USA).

Animal treatments

All animal studies and experimental procedures were approved by the Institutional Animal Care and Use Committee (IACUC) of Peking University Health Science Center, an ethical organization authorized by Beijing Municipal Science and Technology Commission.

NSun2^{+/-} mice were generated from C57BL/6 mice using the Mice TALEN method (Mice NSun2 Gene ID: 28114) in Kangweida Technology Co. Ltd. (Wuhan, China). The constructs used are described in a previous study [18]. Deletion of NSun2 was confirmed by polymerase chain reaction (PCR) and sequence analysis. The primers used for PCR were as follows: CACCTGTCCCGATCACTGAC and ACA GCCTGGTCCTACTACTCA.

Eight-week-old wild-type (WT) or NSun2^{+/-} mice were fed normal chow supplied with either DL-Hcy supplemented (1.8 g/L; Cat. H4628, Sigma-Aldrich, St. Louis, MO, USA) water or normal water for 4 weeks prior to euthanization [12].

As male mice are more susceptible to AAA than female mice, male mice were used for AAA induction [19, 20]. Elastase-induced AAA was performed in mice accordingly [21]. The 10-week-old male mice were subjected to surgery in accordance with the elastase-daubed abdominal aortic aneurysm model. The mice were anesthetized, and the infrarenal aortas were exposed, isolated and wrapped with sterile cotton, followed by the addition and soaking of 40 μ L elastase (68.68 U/mL) for 40 min. Elastase-soaked cotton was then removed, and 0.9% NaCl was used to perfuse the abdominal cavities before suturing.

For the *enpp2*-overexpression model, the abdominal aortas of eight-week-old male WT or NSun2^{+/-} mice were locally transfected with either AAV-NC or AAV-*enpp2* (10^{10} pfu) suspended in 50 μ L 30% Pluronic F-127 gel (Cat. P2443, Sigma-Aldrich, St. Louis, MO, USA) in PBS. Two weeks later, the mice were subjected to surgery to induce AAA as described. The Pluronic gel solution was prepared under sterile conditions and stirred for 12 h at 4 °C. The AAV-Pluronic gel mixture was applied topically to the abdominal aortas and allowed to solidify for 10 min before suturing.

Morphometric, histological and immunofluorescence analysis

The AAA mice were euthanized and perfused through the left ventricle with PBS and fixated with 4% paraformaldehyde through a sternotomy 14 days later. The perivascular connective tissues were removed. The aortas were isolated and fixed on black cloth for photography, and the diameters of the aortas were measured using ImageJ software (National Institutes of Health, Bethesda, ML, USA). Infrarenal abdominal aortas were embedded in OCT compound and cut into serial frozen sections (7- μ m-thick, 70 μ m apart). The aortas were analyzed by a Verhoeff–Von Gieson Staining Kit (Baso Diagnostics Inc., China) for elastin assessment. Elastin degradation was graded on a scale of 1–4, where 1 indicates <25% degradation, 2 indicates 25–50% degradation, 3 indicates 50–75% degradation, and 4 indicates >75% degradation [21].

For immunofluorescent staining, mouse aortic sections were stained with primary antibodies against CD3e (Cat. 99940, Cell Signaling Technology, Danvers, MA), CD19 (Cat. 3574, Cell Signaling Technology, Danvers, MA), α -SMA (Cat. ab32575, Abcam, Cambridge, MA, USA), ATX (Cat. sc-374222, Santa Cruz Biotechnology, Dallas, TX, USA) and CD31 (Cat. A4900, ABclonal, Wuhan, China) overnight at 4 °C, followed by fluorescent secondary antibodies (Alexa Fluor 647/555/488 goat anti-rabbit/mouse/rat IgG) for 1 h at 37 °C. All immunofluorescence analyses were performed at room temperature using a Leica Microsystems instrument (Fluorescence Light DM4000B and Confocal TCS SP8 Microscopes).

Aortic single-cell preparation

The infrarenal abdominal aorta was dissected at 14 days after AAA induction, and the connective and fat tissues surrounding the vessels were removed completely. The aortic tissues were cut into pieces and digested into single cells in 1 mL of 1 \times Aorta Dissociation Enzyme Solution (125 U/mL Collagenase type XI, 60 U/mL Hyaluronidase type 1-s, 60 U/mL DNase I and 450 U/mL Collagenase type I) for 1 h at 37 °C as described previously [22]. All these enzymes were purchased from Sigma-Aldrich (St. Louis, MO, USA). The digested single-cell suspension was used for flow cytometric analysis.

Flow cytometric analysis

To analyze integrin α 4 on the cell surface, T cells were stained with anti-integrin α 4 antibody (Cell Signaling Technology, Danvers, MA) for 30 min on ice, followed by fluorescent secondary antibody (Alexa Fluor 488 goat anti-rabbit IgG) for 1 h. After the unbound antibodies were washed

away, the cells were analyzed using a FACS Calibur flow cytometer (BD Biosciences, Franklin Lakes, NJ, USA) and FlowJo software (Treestar, Ashland, OR, USA).

Analysis of ATX levels in mice and human plasma

The levels of ATX in cell culture supernatants and mouse plasma were measured by enzyme-linked immunosorbent assay (ELISA) kits (Cat. SEC323Mu, CLOUD-CLONE CORP, Houston, USA) according to the manufacturer's instructions. The levels of ATX in human plasma were measured by ELISA kits (Cat. SEC323Hu, CLOUD-CLONE CORP, Houston, USA) according to the manufacturer's instructions.

All clinical samples were obtained at Peking University Third Hospital with informed consent and ethical review committee approval. All experiments were conducted according to the principles expressed in the Declaration of Helsinki. The baseline characteristics of the patients are summarized in Table S1.

Cell isolation and culture

Splenic T cells from mouse spleen were purified by positive selection with magnetic microbeads against CD90.2 according to the manufacturer's protocol (Miltenyi Biotec, Bergisch Gladbach, Germany). The plates that cultured purified splenic T cells were precoated with anti-CD3 antibody (as basic stimulation, 1 µg/mL, BD Biosciences, Franklin Lakes, NJ, USA) overnight.

Human umbilical vein endothelial cells (HUVECs, from Dr. Lei Wang, Institute of Biophysics, CAS), Jurkat T cells (purchased from ATCC, Manassas, VA, USA) and purified mouse splenic T cells were cultured in RPMI 1640 media (Gibco, Gaithersburg, MD, USA) supplemented with 10% fetal bovine serum (Gemini Bio-Products, West Sacramento, CA, USA) and penicillin/streptomycin (Gibco, Gaithersburg, MD, USA). All cells were cultured at 37 °C in a humidified atmosphere containing 5% CO₂.

T cell chemotaxis assay

Jurkat T cells (10⁶) were added to the upper chamber of Transwells (Cat. 3421, Corning, NY, USA). For induction of chemokinesis, the indicated concentrations of ATX were added to the upper chamber of Transwells. For induction of chemotaxis, the indicated concentrations of ATX were added to the lower chamber of Transwells. CXCL12 (0.5 µg/mL or 5 µg/mL) was added to the lower chamber as a positive control [23]. After 3 h of incubation at 37 °C [24], the cells migrated to the lower chamber were quantified by cell-count boards.

T cell adhesion assay

Jurkat T cells were fluorescently labeled with 5 ng/mL calcein-AM in complete RPMI 1640 medium for 10 min at 37 °C in the dark. Then, HUVECs were pretreated with TNF-α (tumor necrosis factor α; 4 ng/mL) for 24 h in 6-well plates, followed by coculture with labeled Jurkat T cells (1 × 10⁶ cells/well) for 30 min. Recombinant soluble human ICAM-1 (1 µg/mL or 10 µg/mL) was coated on the plates by overnight incubation at 4 °C, or MnCl₂ (1 mM or 10 mM) was added to the labeled Jurkat T cell suspension as a positive control [25]. Labeled Jurkat T cells was added to 6-well plates without HUVECs as a negative control. After the non-adherent cells were removed by washing with PBS 3 times, the adherent Jurkat T cells were evaluated using a fluorescence microscope (Leica, Wetzlar, Germany). Six random fields per well were imaged and subsequently quantified by ImageJ software (National Institutes of Health, Bethesda, ML, USA).

In vivo T cell migration assay

CD3⁺ T cells from WT mice were labeled with CFSE (Cat. C1157, Invitrogen, Waltham, MA, USA) according to the manufacturer's instructions. The effect of the CFSE label itself on T cell viability was tested using the Annexin V-FITC/PI Apoptosis Detection Kit (Cat. CTK007-100, M&C Gene Technology, Beijing, China) after labeling for 16 h [26]. A total of 10⁷ labeled cells were intravenously injected into one recipient WT or NSun2^{+/-} mouse whose infrarenal abdominal aorta had been treated with elastase for 3 days. 16 h later, the aortas were digested into single cells as described above and the proportions of CFSE-labeled donor cells in infrarenal abdominal aortas were measured by flow cytometry.

Western blotting

Cells or tissues were lysed in cold RIPA buffer to extract the total protein. Protein concentrations were evaluated using the BCA Protein Assay Kit (Thermo Scientific, Waltham, MA). Equal amounts of total protein were resolved by 10% SDS-PAGE and transferred onto polyvinylidene difluoride membranes (Millipore, Billerica, MA, USA). The membranes were incubated with primary antibodies against ATX (Santa Cruz Biotechnology, Dallas, TX, USA), integrin α4 (Cell Signaling Technology, Danvers, MA, USA), p-FAK (Cell Signaling Technology, Danvers, MA, USA), FAK (Cell Signaling Technology, Danvers, MA, USA), p-Src (Cell Signaling Technology, Danvers, MA, USA), Src (Cell Signaling Technology, Danvers, MA, USA), RhoA (Cytoskeleton, Denver, CO, USA), β-actin (ABclonal, Wuhan, China) and appropriate HRP-conjugated secondary

antibodies (Abclonal, Wuhan, China). The blots were visualized by an Odyssey infrared imaging system (LI-COR Biosciences, Lincoln, NE) after coating with Immobilon Western Chemiluminescent HRP Substrate (Millipore corporation, MA, USA).

Co-immunoprecipitation

T cells stimulated with or without ATX were lysed in cold RIPA buffer, incubated with ATX antibody, and immunoprecipitated with protein A/G agarose beads (Santa Cruz Biotechnology, Dallas, TX, USA). Mouse IgG (sc-2025, Santa Cruz Biotechnology, Dallas, TX, USA) was used as a negative control. The precipitated proteins were resolved by 10% SDS-PAGE as described above and then incubated with an antibody against integrin $\alpha 4$. β -actin was detected by immunoblotting as a loading control.

Rho GTPase activation assay

Rho GTPase activation was analyzed by the RhoA Pull-down Activation Assay Biochem Kit (bead pull-down format) (Cat. BK036, Cytoskeleton, Denver, CO, USA) according to the manufacturer's instructions.

Real-time polymerase chain reaction

Total RNA was isolated from infrarenal abdominal aortas, HUVECs and T cells using TRIzol reagent (Invitrogen, Carlsbad, CA, USA) and reverse transcribed to cDNA using $5 \times$ All-In-One RT MasterMix (ABM Inc, Vancouver, Canada). Real-time polymerase chain reaction (PCR) amplification was performed using $2 \times$ RealStar Green Power Mixture (GenStar, San Diego, USA) and recorded using the Mx3000 Multiplex Quantitative PCR System (Stratagene, La Jolla, CA, USA). The target mRNA levels were normalized to the level of β -actin mRNA. The primer sequences used for real-time PCR analyses were listed in Table S2.

mRNA half-life measurement

To measure the half-life of endogenous *enpp2* mRNA, actinomycin D ($2 \mu\text{g}/\text{mL}$, Sigma-Aldrich, St. Louis, MO, USA) was added to the cell culture medium. Total RNA was prepared at the indicated times and subjected to real-time PCR analysis using *enpp2*-specific primers.

RNA sequencing analysis (RNA-seq)

Total RNA from HUVECs was isolated as described above. A total amount of $3 \mu\text{g}$ RNA per sample was used as input material for RNA sample preparation. Library construction and RNA sequencing were performed by the Novogene

Bioinformatics Institute (Beijing, China). Sequencing libraries were generated using the NEBNext UltraTM RNA Library Prep Kit (New England Biolabs, Ipswich, MA, USA) for the Illumina system following the manufacturer's instructions. Reference genome and gene model annotation files were downloaded from the genome website directly. The index of the reference genome was built using Hisat2 (v2.0.5). The mapped reads of each sample were assembled by StringTie (v1.3.3b) in a reference-based approach. Differential expression analysis of two groups was performed using the DESeq 2 R package (1.16.1). Genes with an adjusted P value < 0.05 found by DESeq 2 were assigned as differentially expressed.

Statistical analysis

All data are shown as the mean \pm SEM unless otherwise stated. GraphPad Prism software was used for data analysis. Statistical analysis was performed with one-way or two-way ANOVA followed by Tukey's test for multiple comparisons and with unpaired Student's t test for comparisons between two groups. A value of $P < 0.05$ was considered statistically significant.

Results

NSun2 deficiency attenuates HHcy-aggravated AAA in mice

Recruitment of leukocytes to the aortic wall plays a key role in AAA progression [27]. In rats, we have demonstrated that the RNA methyltransferase NSun2 upregulates ICAM-1 expression in vascular endothelial cells, thereby increasing the adhesion of leukocytes to the endothelium in arteriosclerosis [8]. To explore the potential role of NSun2 and especially the NSun2-mediated interaction between leukocytes and the endothelium in a murine AAA experimental model, we first generated NSun2-knockout mice using TALEN technology. Because the homozygous knockout mice (NSun2^{-/-}) died during the embryonic period, we used heterozygous knockdown mice (NSun2^{+/-}) to perform the following experiments. The knockdown of NSun2 was confirmed by sequence analysis (Fig. S1a). The expression of NSun2 was significantly decreased in various tissues of NSun2^{+/-} mice (Fig. S1b), further confirming the successful knockdown of NSun2. NSun2^{+/-} mice exhibited weight loss and no obvious abnormalities in terms of total cholesterol, triglyceride levels or proportion of blood cells compared with the wild-type littermates (Table S3).

To examine the role of NSun2 in elastase-induced and HHcy-accelerated AAA, we used WT and NSun2^{+/-} mice, which were fed a normal chow diet and given drinking water

supplemented with or without 1.8 g/L Hcy for 2 weeks, to develop an elastase-induced AAA model. Two weeks after elastase induction, we observed a significant expansion of the infrarenal abdominal aorta in WT mice (0.93 ± 0.03 mm in the saline group and 1.65 ± 0.23 mm in the elastase group; Fig. 1a, b). This process was aggravated by HHcy (2.38 ± 0.13 mm; Fig. 1a, b). NSun2 knockdown markedly reduced the expansion of the infrarenal abdominal aorta, and there was no obvious aortic aneurysm in both NSun2^{+/-} groups treated with or without HHcy (1.06 ± 0.10 mm in the elastase group and 1.38 ± 0.13 mm in the HHcy plus elastase group; Fig. 1a, b). Consistent results were obtained from ultrasonography (Fig. 1c). Notably, in WT mice, the incidence of AAA in the HHcy plus elastase group was 100% (8/8), which is significantly higher than that in the elastase alone group (62.5%, 5/8), while the incidence of AAA was decreased dramatically in both groups with or without HHcy in NSun2^{+/-} mice (12.5%, 1/8 in the elastase group and 37.5%, 3/8 in the HHcy plus elastase group; Fig. 1d). Moreover, Verhoeff–Van Gieson staining showed that NSun2 knockdown also significantly inhibited elastin degradation in elastase-induced and HHcy-aggravated AAA (Fig. 1e). These results indicate that the development of elastase-induced and HHcy-aggravated AAA is attenuated in NSun2^{+/-} mice.

NSun2 deficiency reduces T cell infiltration in the aortic wall of HHcy-aggravated AAA

The above data suggested that NSun2 may be involved in murine AAA development. Afterwards, we further investigated the potential mechanisms by which NSun2 mediated AAA formation. As the early pathologic stage of AAA, various inflammatory cell infiltrations in the vessel wall may normally be first investigated. By immunofluorescent staining, we found that the number of T cells recruited to the aortic wall induced by elastase and aggravated by HHcy was markedly decreased in NSun2^{+/-} mice (Fig. 2a). However, NSun2 deficiency did not significantly affect the infiltration of B cells in AAA (Fig. S2). We next collected elastase-treated infrarenal abdominal aortas with or without HHcy groups and then digested them into single-cell suspensions for the following flow cytometric assay to confirm the T cell number in those vascular samples. As anticipated, NSun2 deficiency significantly inhibited the accumulation of CD3⁺ T cells in the infrarenal abdominal aortic wall during elastase-induced and HHcy-accelerated AAA formation ($0.05 \pm 0.02\%$ in the saline WT group, $0.85 \pm 0.07\%$ in the elastase WT group, $1.57 \pm 0.12\%$ in the HHcy plus elastase WT group, $0.06 \pm 0.02\%$ in the saline NSun2^{+/-} group, $0.21 \pm 0.05\%$ in the elastase NSun2^{+/-} group, $0.50 \pm 0.15\%$ in the HHcy plus elastase NSun2^{+/-} group; Fig. 2b).

The T cell number in lesions was specifically decreased in NSun2^{+/-} mice, which may be one of the major causes for the decreased AAA incidence and suggests the pivotal role of T cells in AAA development as well. To confirm this phenomenon by inducing T cell depletion in vivo, recipient C57BL/6J mice were intraperitoneally injected with anti-CD3 ϵ F(ab')₂ fragments for six consecutive days as described [28], followed by an AAA-inducing operation (Fig. S3a). We next assessed the formation of elastase-induced AAA in these mice. The maximal diameters of the infrarenal abdominal aortas of the anti-CD3 ϵ F(ab')₂-treated mice were much smaller than those of the IgG isotype control recipient mice after elastase induction (Fig. 2c, d). Verhoeff–Van Gieson staining demonstrated that elastin degradation in elastase-induced AAA was inhibited in anti-CD3 ϵ -treated mice (Fig. 2e, f). These data confirmed the critical role of T cells in AAA formation.

Furthermore, we performed adoptive transfer experiments. A total of 10^7 CFSE-labeled WT CD3⁺ T cells were transferred into recipient WT or NSun2^{+/-} mice, whose infrarenal abdominal aortas had been pretreated with elastase for 3 days (Fig. S3b). CFSE labeling per se did not affect cell apoptosis and necrosis (data not shown). Flow cytometric assays showed that 16 h after transfer, the percentages of CFSE-labeled T cells in the infrarenal abdominal aortas of recipient NSun2^{+/-} mice were significantly lower than those of recipient WT mice (Fig. 2g), suggesting that the decreased T cell number in AAA lesions of NSun2^{+/-} mice shown above may be partly due to NSun2 deficiency in aortas.

Hcy upregulates endothelial autotaxin (ATX) expression and secretion in vitro and in vivo

To explore the potential regulatory targets of NSun2, HUVECs were treated with or without Hcy (100 μ M) for 24 h and then subjected to RNA sequencing analysis (RNA-seq). Interestingly, prominent changes were observed in metabolic enzymes involved in the PC-LPC-LPA pathway, especially *enpp2*, known as the lysophospholipase ATX gene (Fig. 3a). In the verification experiments, Hcy (100 μ M) treatment for 24 h markedly enhanced ATX protein (Fig. 3b) and mRNA expression (Fig. 3c) in HUVECs, accompanied by increased ATX levels in the culture supernatants (Fig. 3d), without altering the half-life of ATX mRNA (Fig. 3e). In parallel, the plasma level of ATX was markedly elevated in HHcy mice compared with the control mice (Fig. 3f). To further investigate the relative translational significance of these data, we preliminarily analyzed the ATX level of human plasma during the health physical examination, the baseline characteristics of which are summarized in Table S1. The plasma ATX level was positively correlated with the Hcy

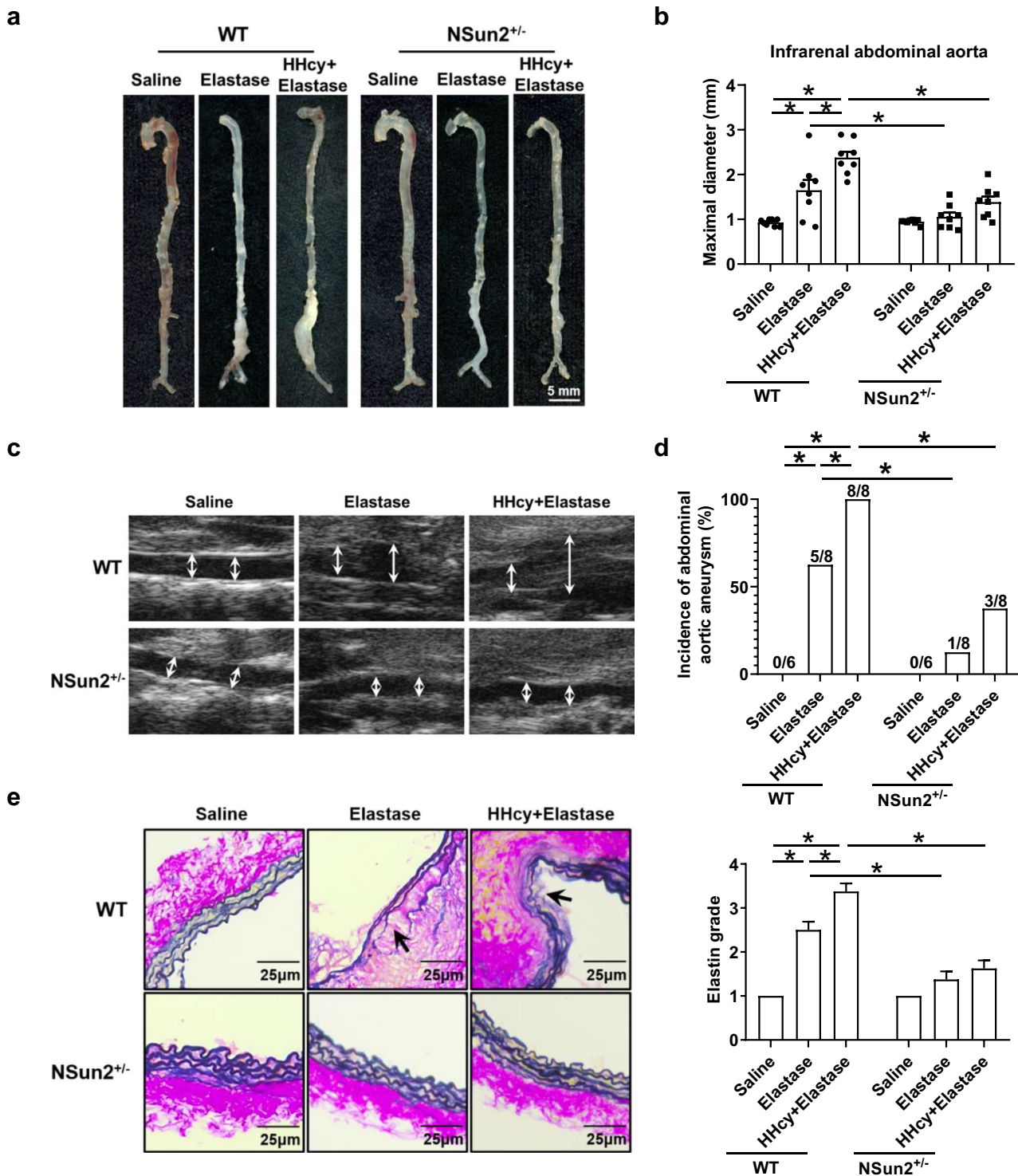


Fig. 1 NOP2/Sun domain family, member 2 (NSun2) deficiency attenuates HHcy-aggravated abdominal aortic aneurysm (AAA) in mice. Infrarenal abdominal aortas of 10- to 11-week-old wild-type (WT) and NSun2^{+/-} mice were treated with saline or elastase to induce abdominal aortic aneurysm after the mice were fed a normal chow diet and given drinking water supplemented with or without 1.8 g/L Hcy for 2 weeks. **a–c** Representative photographs (**a**) quantification of maximal diameters (**b**) and representative images (**c**)

of ultrasonography of infrarenal abdominal aortas ($n=6-8$). **d** Incidence of abdominal aortic aneurysm. **e** Representative Verhoeff–Van Gieson staining and statistical analysis of elastin degradation in the infrarenal abdominal aortas ($n=8$). Scale bar, 25 μ m. Data shown are mean \pm SEM. * $P < 0.05$, by two-way analysis of variance (ANOVA) followed by Tukey’s test for multiple comparisons (**b**, **e**) or Fisher’s exact test (**d**)

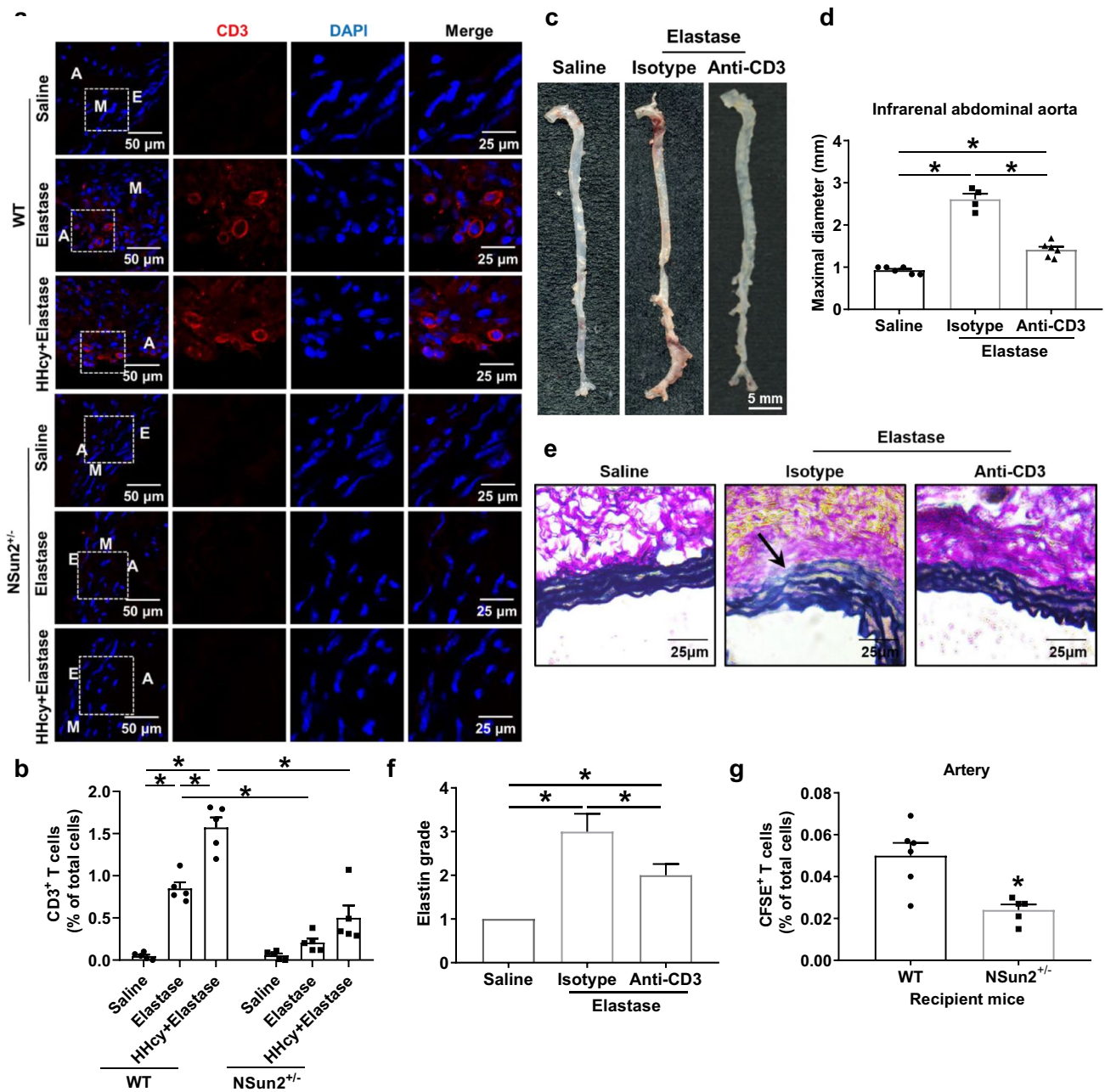


Fig. 2 NSun2 deficiency reduces T cell infiltration in aortic wall of HHcy-aggravated AAA. **a, b** Infrarenal abdominal aortas of 10- to 11-week-old WT and NSun2^{+/-} mice were treated with saline or elastase to induce abdominal aortic aneurysm after the mice were fed a normal chow diet and given drinking water supplemented with or without 1.8 g/L Hcy for 2 weeks. **a** Representative immunofluorescent staining of CD3⁺ T cells of infrarenal abdominal aortas. Scale bar, 25 μ m. **b** Quantification of CD3⁺ T cells by flow cytometry of infrarenal abdominal aortas ($n=5$). **c, d** Representative photographs (**c**) and quantification (**d**) of maximal diameters of infrarenal abdominal aortas (Saline, $n=6$; Elastase + isotype, $n=4$; Elastase + anti-CD3, $n=6$). **e, f** Representative Verhoeff–Van Gieson staining (**e**) and

statistical analysis (**f**) of elastin degradation in the infrarenal abdominal aortas (Saline, $n=6$; Elastase + isotype, $n=4$; Elastase + anti-CD3, $n=6$). Scale bar, 25 μ m. **g** After adoptive transfer of CFSE-labeled WT donor T cells into recipient WT or NSun2^{+/-} mice whose infrarenal abdominal aortas were treated with elastase for 3 days, the proportions of WT donor T cells in the infrarenal abdominal aortas were analyzed by flow cytometry (WT, $n=6$; NSun2^{+/-}, $n=5$). Data shown are mean \pm SEM. * $P < 0.05$, by two-way ANOVA followed by Tukey's test for multiple comparisons (**b**), one-way ANOVA followed by Tukey's test for multiple comparisons (**d, f**) or unpaired Student *t* test (**g**). *E* endothelium, *M* tunica media, *A* tunica adventitia

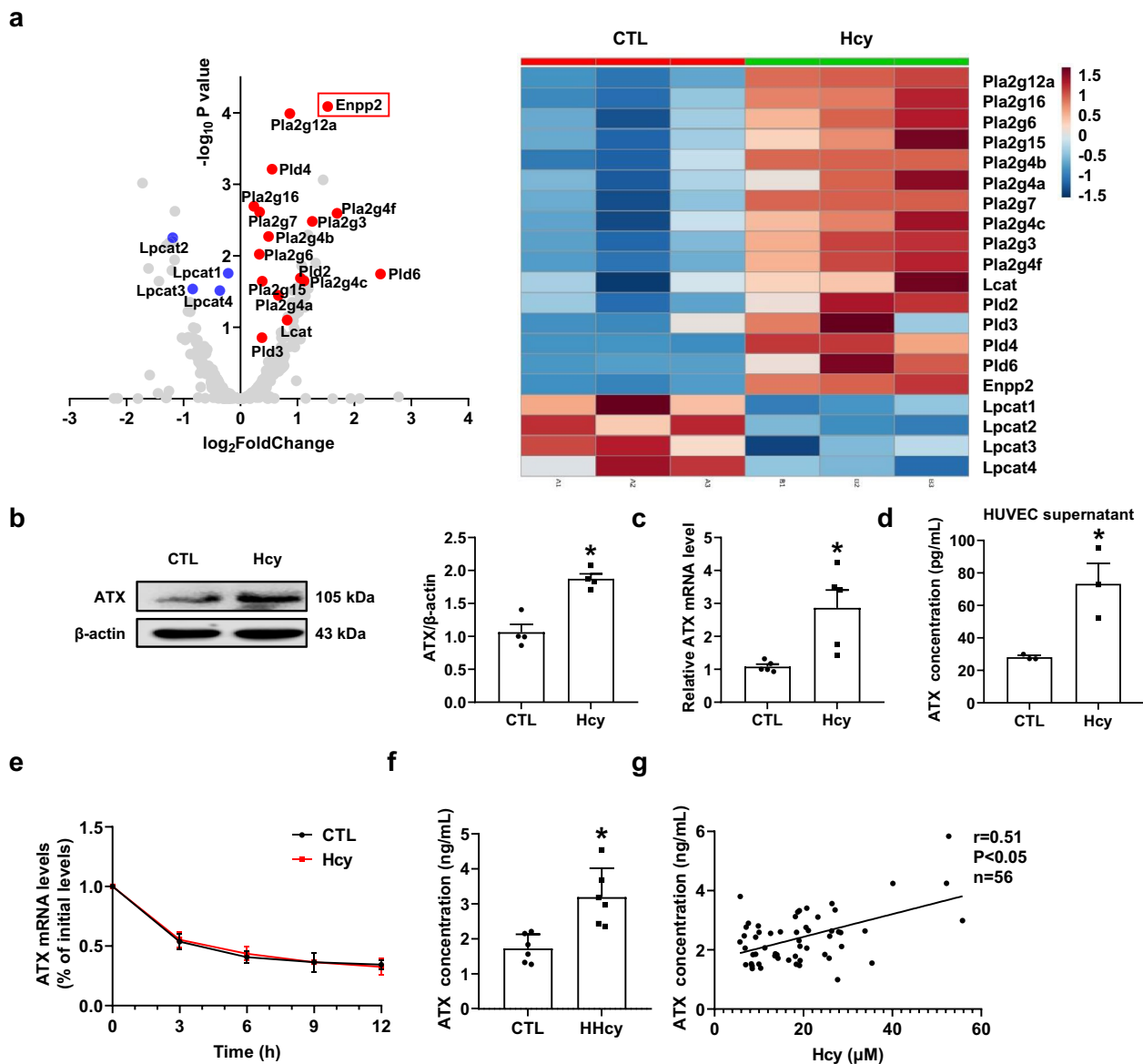


Fig. 3 Hcy upregulates endothelial autotaxin (ATX) expression and secretion in vitro and in vivo. **a** Volcano plots and heat map showing differentially expressed metabolizing enzyme genes in metabolic pathways for LPC after Hcy (100 μ M) stimulation for 24 h. **b–d** Human umbilical vein endothelial cells (HUVECs) were stimulated with or without Hcy (100 μ M) for 24 h. **b** Representative Western blot analysis of ATX expression after Hcy stimulation for 24 h ($n = 4$). **c** Real-time polymerase chain reaction (PCR) quantification of ATX mRNA levels after Hcy stimulation for 24 h ($n = 5$). **d** ATX

levels in the culture supernatants after Hcy stimulation for 24 h were measured via ELISA ($n = 3$). **e** Real-time PCR quantification of ATX mRNA levels of at 0 h, 3 h, 6 h, 9 h, 12 h after adding Hcy (100 μ M) and actinomycin D (2 μ g/mL) into the cell culture medium ($n = 3$). **f** Plasma ATX levels of control or HHcy C57BL/6J mice were measured via ELISA ($n = 6$). **g** Plasma ATX levels of patients were measured via ELISA ($n = 56$). Data shown are mean \pm SEM. * $P < 0.05$, by unpaired Student *t* test (**b–d**, **f**)

concentration (Fig. 3g). Plasma ATX can reach over 4 ng/mL when the Hcy concentration is beyond 40 μ M. These results suggest that Hcy upregulates both ATX protein expression and secretion from the endothelium in vitro, as well as plasma levels of both humans and mice in vivo.

NSun2 deficiency reduces ATX upregulation in the endothelium and plasma of HHcy-aggravated AAA

ATX is widely expressed in the brain, ovary, lung, intestine and kidney [29]. Lymph nodes and high endothelial

cells have abundant expression of ATX [24]. In the present study, ATX expression in vessels of AAA was tested first in WT and NSun2^{+/-} mice. The total expression of ATX in infrarenal abdominal aortas was constitutive and significantly elevated after elastase induction at both the protein and mRNA levels (Fig. 4a, b). Notably, the elevation of the

ATX protein level, but not the mRNA level, was abrogated in NSun2^{+/-} mice (Fig. 4a, b). These results indicate that NSun2 deficiency downregulates ATX protein expression in AAA vascular lesions.

We next explored the potential cellular source of ATX in AAA vessels. *En face* staining of ATX expression in the

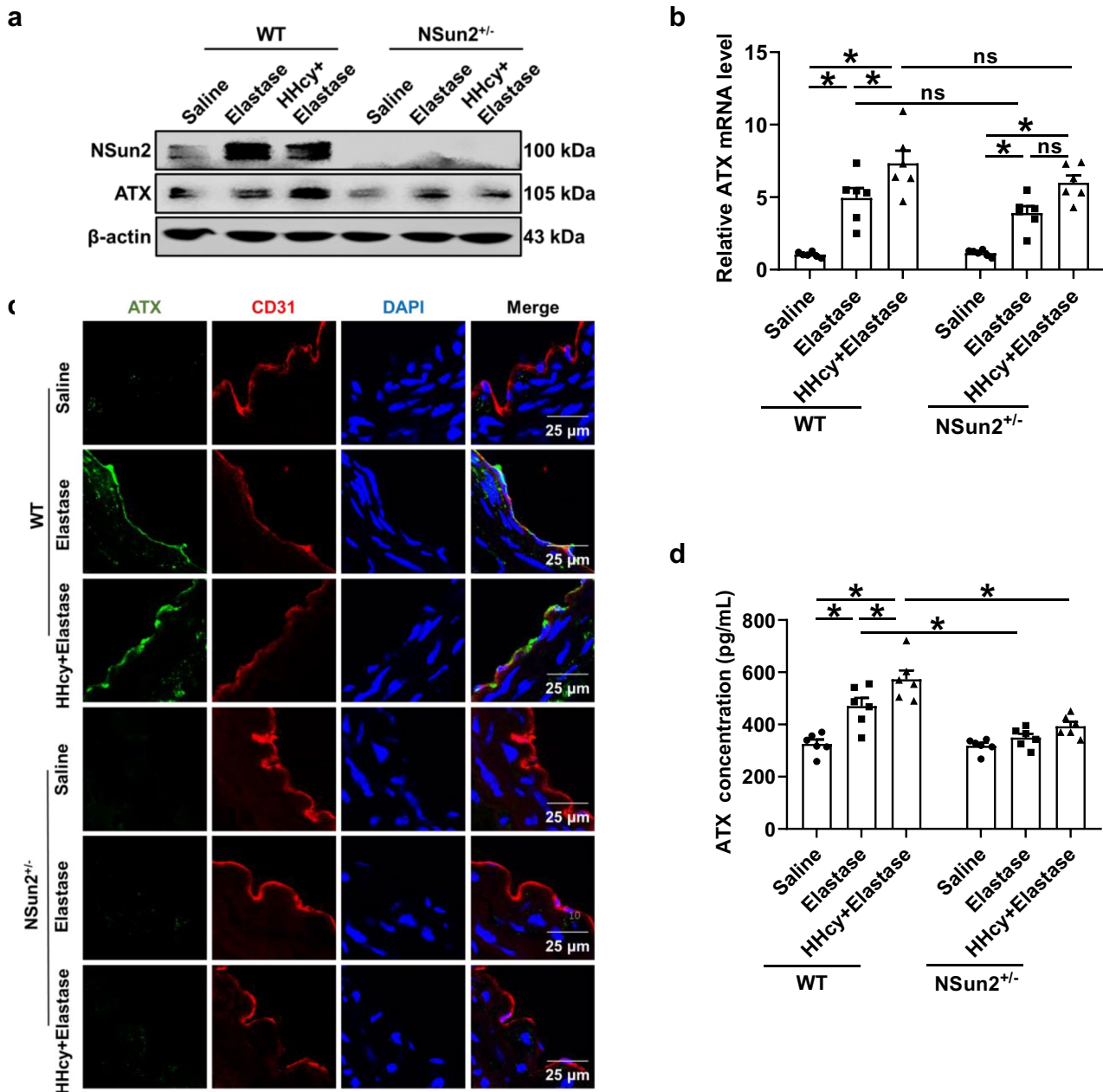


Fig. 4 NSun2 deficiency reduces ATX upregulation in endothelium and plasma of HHcy-aggravated AAA. Infrarenal abdominal aortas of 10- to 11-week-old WT and NSun2^{+/-} mice were treated with saline or elastase to induce abdominal aortic aneurysm after the mice were fed a normal chow diet and given drinking water supplemented with or without 1.8 g/L Hcy for 2 weeks. **a** Representative Western blot analysis of ATX expression in infrarenal abdominal aortas. **b** Real-

time PCR quantification of ATX mRNA levels in infrarenal abdominal aortas ($n=6$). **c** Representative immunofluorescent staining of ATX expression in endothelial cells (CD31 positive) in infrarenal abdominal aortas. Scale bar, 25 μ m. **d** Plasma ATX levels were measured via ELISA ($n=6$). Data shown are mean \pm SEM. * $P < 0.05$, by two-way ANOVA followed by Tukey's test for multiple comparisons (**b**, **d**). *ns* no significance

endothelial layer of elastase-treated infrarenal abdominal aortas showed that ATX was highly expressed in CD31-positive endothelial cells (Fig. S4a). However, immunofluorescent staining data indicated that there is probably no ATX expression in CD3-positive T cells (Fig. S4b) or SMA-positive vascular smooth muscle cells (Fig. S4c) in the sections of elastase-treated infrarenal abdominal aorta. Meanwhile, immunofluorescent staining of infrarenal abdominal aortas confirmed the expression of ATX in endothelial cells and the loss of ATX expression in NSun2^{+/-} mice (Fig. 4c). A similar decreasing tendency was obtained in the plasma ATX levels of NSun2^{+/-} AAA mice (Fig. 4d). More importantly, HHcy-increased endothelial ATX expression (Fig. 4c), and plasma ATX elevation were downregulated significantly in NSun^{+/-} mice as well (Fig. 4d), which was consistent with changes in aortic ATX protein expression (Fig. 4a). These results indicate that NSun2 can modulate ATX protein expression and secretion, and the vascular endothelium may be an important source of ATX during elastase-induced and HHcy-aggravated AAA formation.

ATX induces T cell adhesion by binding to integrin $\alpha 4$ and activating the FAK/Src-RhoA signal pathway in vitro

To explore the potential interaction between the ATX and T cells during AAA formation, we investigated the influence of ATX and Hcy on T cell migration or adhesion to endothelial cells in vitro. First, to determine whether ATX had motility-enhancing or chemotactic effects on T cells, we performed a Transwell migration assay using Jurkat T cells as reported [24]. Increased migration of Jurkat T cells was observed when ATX (0.5–2 nM) was added to the upper chamber but not in the lower chamber (Fig. 5a), suggesting that ATX could increase the chemokinesis of T cells. CXCL12 was added to the lower chamber as a positive control. We next labeled the Jurkat T cells with calcein-AM and cocultured them with HUVECs for 30 min. And recombinant soluble human ICAM-1 (sICAM-1) was coated on the plates, or MnCl₂ was added in the labeled Jurkat T cells suspension as a positive control. Confocal microscopy data showed that ATX (0.5–5 nM) pretreatment promoted the adhesion of Jurkat T cells to HUVECs in a dose-dependent manner (Fig. 5b).

Integrin $\alpha 4$ or $\beta 1$ on T cells may be involved in ATX-promoted cell adhesion [24]. We first tested whether ATX regulated the expression of various integrins on T cells. The results showed that ATX significantly upregulated the mRNA expression of integrin $\alpha 4$ but not any other integrin, such as αL , $\beta 1$ or $\beta 2$, whereas integrin $\beta 7$ also showed a tendency for increased expression (Fig. 5c). Consistent with the mRNA expression results, ATX (0.5–5 nM) dose-dependently upregulated the protein expression of integrin

$\alpha 4$ in T cells, as indicated by flow cytometric assay (Fig. 5d). Figure 5e is a typical fluorescent image of increased integrin $\alpha 4$ expression in T cells by ATX (0.5 nM) treatment. Furthermore, anti-CD49d mAb, an integrin $\alpha 4$ neutralizing antibody, significantly inhibited the adhesion of T cells to HUVECs induced by ATX or Hcy (Fig. 5f).

A co-immunoprecipitation assay with an antibody specific to ATX demonstrated that ATX bound to integrin $\alpha 4$ directly (Fig. 6a). As reported, FAK, Src family kinases and the Rho-family of GTPases (RhoA, Rac1, and Cdc42), which are crucial regulators of intracellular signal pathways, can be activated by integrins and promote cell adhesion and transmigration [30, 31]. In the present study, ATX upregulated the phosphorylation of FAK-Tyr397 and Src-Tyr416 and activated the RhoA signaling pathway in T cells (Fig. 6b). RGDS (20 nM), an integrin inhibitor, effectively inhibited the activation of FAK and Src induced by ATX (Fig. 6c). To further confirm the effects of endothelial cell-secreted ATX under Hcy stimulation, the supernatants from HUVECs stimulated with or without Hcy (100 μ M) for 24 h were transferred to T cells pretreated with or without the ATX lysoPLD activity inhibitor HA130 (1 μ M) for 24 h. The data showed that HA130 suppressed the activation of FAK and Src in T cells caused by Hcy-stimulated HUVEC supernatant (Fig. 6d). These results indicate that ATX induces T cell migration and adhesion via binding to integrin $\alpha 4$ and activating the downstream FAK/Src signaling pathway.

Overexpression of ATX in aortas aggravates AAA development in NSun2^{+/-} mice

To further confirm that ATX mediates NSun2-regulated AAA formation in vivo, we designed adeno-associated virus (AAV) to overexpress ATX (*enpp2*) in the elastase-treated infrarenal abdominal aortas of WT and NSun2^{+/-} mice. AAV-NC or AAV-*enpp2* (10¹⁰ pfu) was applied to the elastase-induced abdominal aortas. Successful overexpression of ATX in infrarenal abdominal aortas was confirmed by western blotting and real-time PCR quantification (Fig. 7a, b). ATX overexpression markedly aggravated the maximal diameters of infrarenal abdominal aortas both in WT mice (1.49 \pm 0.09 mm in the AAV-NC group and 1.95 \pm 0.08 mm in the AAV-*enpp2* group) and in NSun2^{+/-} mice (0.99 \pm 0.06 mm in the AAV-NC group and 1.43 \pm 0.13 mm in the AAV-*enpp2* group; Fig. 7c, d). Verhoeff–Van Gieson staining showed that ATX overexpression aggravated elastin degradation in WT and NSun2^{+/-} mice (Fig. 7e). In these mice, endothelial ATX expression was upregulated after AAV-*enpp2* transfection (Fig. 7f), accompanied by more CD3⁺ T cell infiltration (Fig. 7g). Therefore, NSun2 mediates AAA development by promoting ATX protein expression and secretion in the endothelium, subsequently inducing T cell migration and adhesion (Fig. 8).

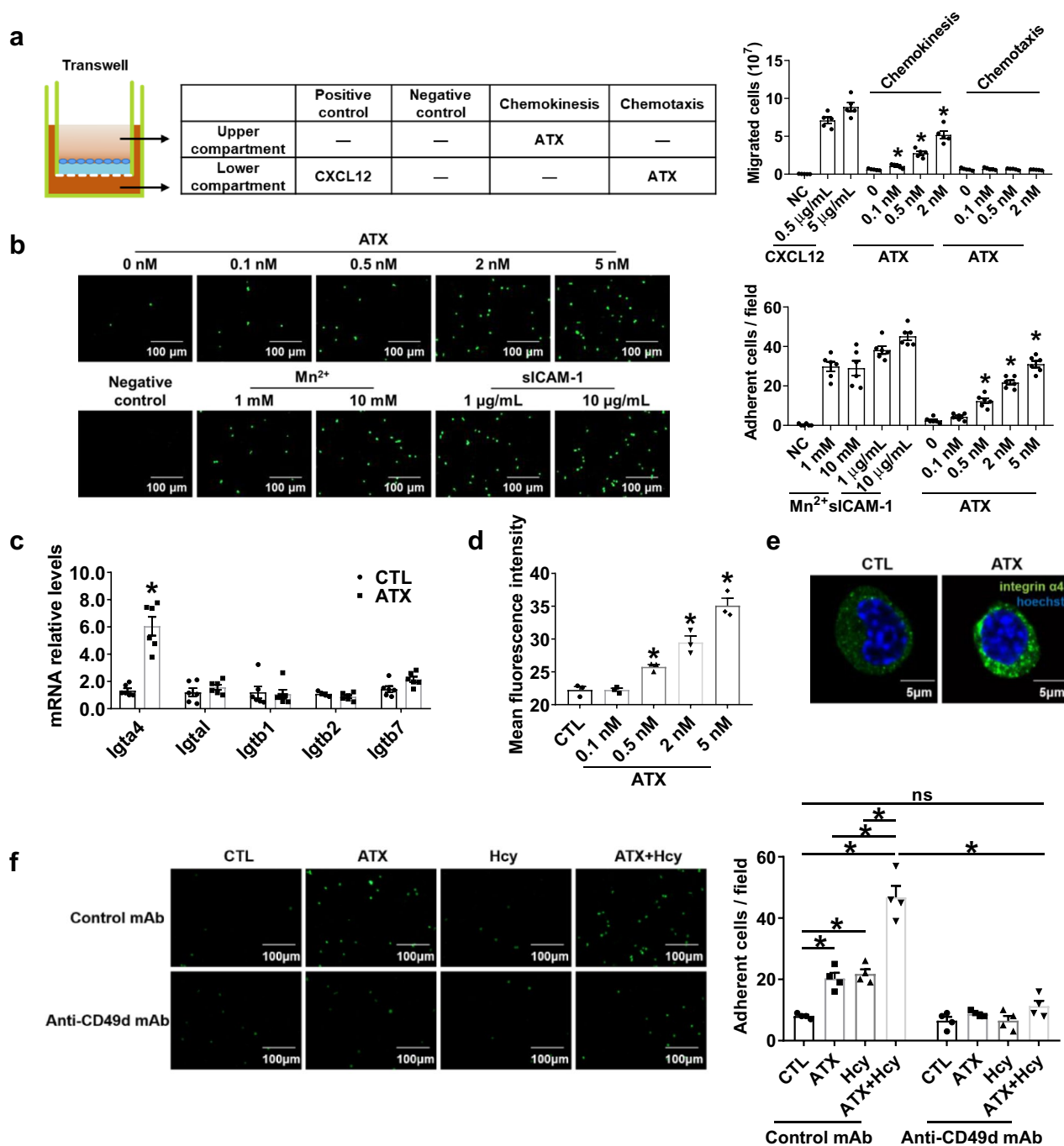


Fig. 5 ATX induces chemokinesis and adhesion of T cells via activating integrin $\alpha 4$. **a** Transwell migration assay of Jurkat T cells added to the upper chamber with ATX added either to the same chamber (to induce chemokinesis) or to the lower chamber (to induce chemotaxis); after 3 h of incubation at 37 °C, cells that had migrated to the bottom chamber were quantified ($n=5$). $*P<0.05$, compared with 0 nM ATX. **b** Representative photographs and quantification of the adhesion of calcein-AM-labeled Jurkat T cells to HUVECs after coculture with or without indicated concentrations of ATX for 0.5 h ($n=6$). Scale bar, 100 μm . $*P<0.05$, compared with 0 nM ATX. **c–e, g–j** Splenic T cells purified from C57BL/6J mice were cultured in vitro with or without ATX for 0.5 h. **c** Real-time PCR quantification of mRNA levels of T cell integrin treated with ATX (0.5 nM) for

0.5 h ($n=6$). **d** Quantification of activated integrin $\alpha 4$ in T cells after ATX stimulation for 0.5 h by flow cytometry ($n=3$). **e** Representative immunofluorescent staining of integrin $\alpha 4$ after ATX (0.5 nM) stimulation for 0.5 h. Scale bar, 5 μm . **f** Representative photographs and quantification of the adhesion of calcein-AM-labeled Jurkat T cells to HUVECs after coculture for 0.5 h with or without ATX (0.5 nM) and Hcy (100 μM) and with an equal amount of mouse IgG or integrin $\alpha 4$ neutralizing antibody anti-CD49d mAb (10 $\mu\text{g}/\text{mL}$) ($n=4$). Scale bar, 100 μm . Data shown are mean \pm SEM. $*P<0.05$, by one-way ANOVA followed by Tukey's test for multiple comparisons (**a, b, d**), unpaired Student *t* test (**c**), or two-way ANOVA followed by Tukey's test for multiple comparisons (**f**). *ns* no significance

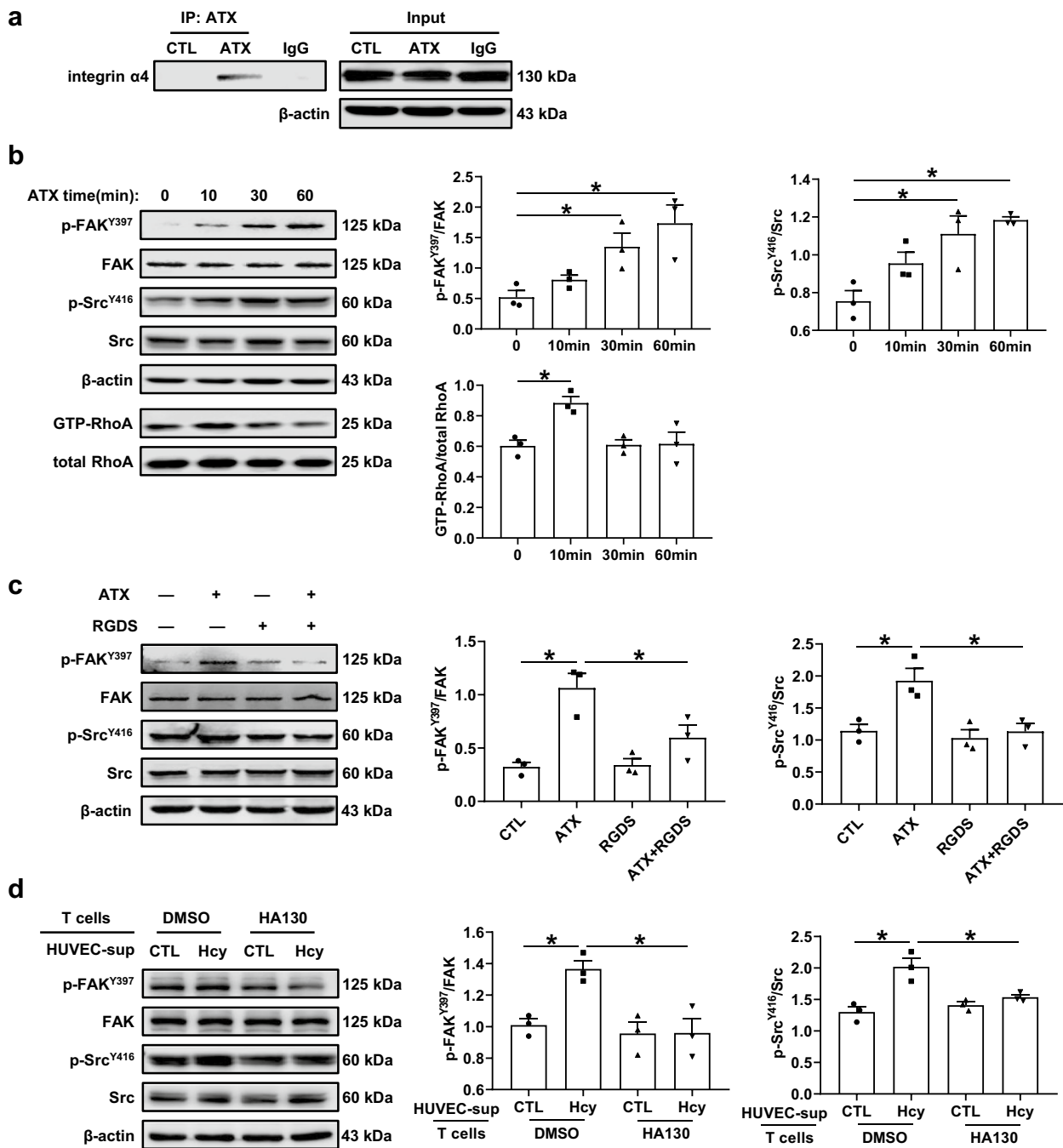


Fig. 6 ATX binds to integrin $\alpha 4$ and activates FAK/Src-RhoA signal pathway. **a** T cells stimulated with or without ATX (0.5 nM) for 0.5 h. Co-immunoprecipitation of ATX with integrin $\alpha 4$ in T cells ($n=3$). **b** Representative Western blot analysis and quantification of FAK (focal adhesion kinase), Src and RhoA activation in T cells treated with ATX (0.5 nM) for various periods ($n=3$). **c** Representative Western blot analysis and quantification of FAK and Src activation in T cells treated with or without ATX (0.5 nM) and pretreated with

or without RGDS (20 nM) for 0.5 h ($n=3$). **d** Representative Western blot analysis and quantification of FAK and Src activation in T cells. Supernatant (sup) from HUVECs stimulated with or without Hcy (100 μ M) for 24 h were transferred to T cell and cultured with or without HA130 (1 μ M) for 24 h ($n=3$). Data shown are mean \pm SEM. $*P < 0.05$, by one-way ANOVA followed by Tukey's test for multiple comparisons (**b**), or two-way ANOVA followed by Tukey's test for multiple comparisons (**c**, **d**)

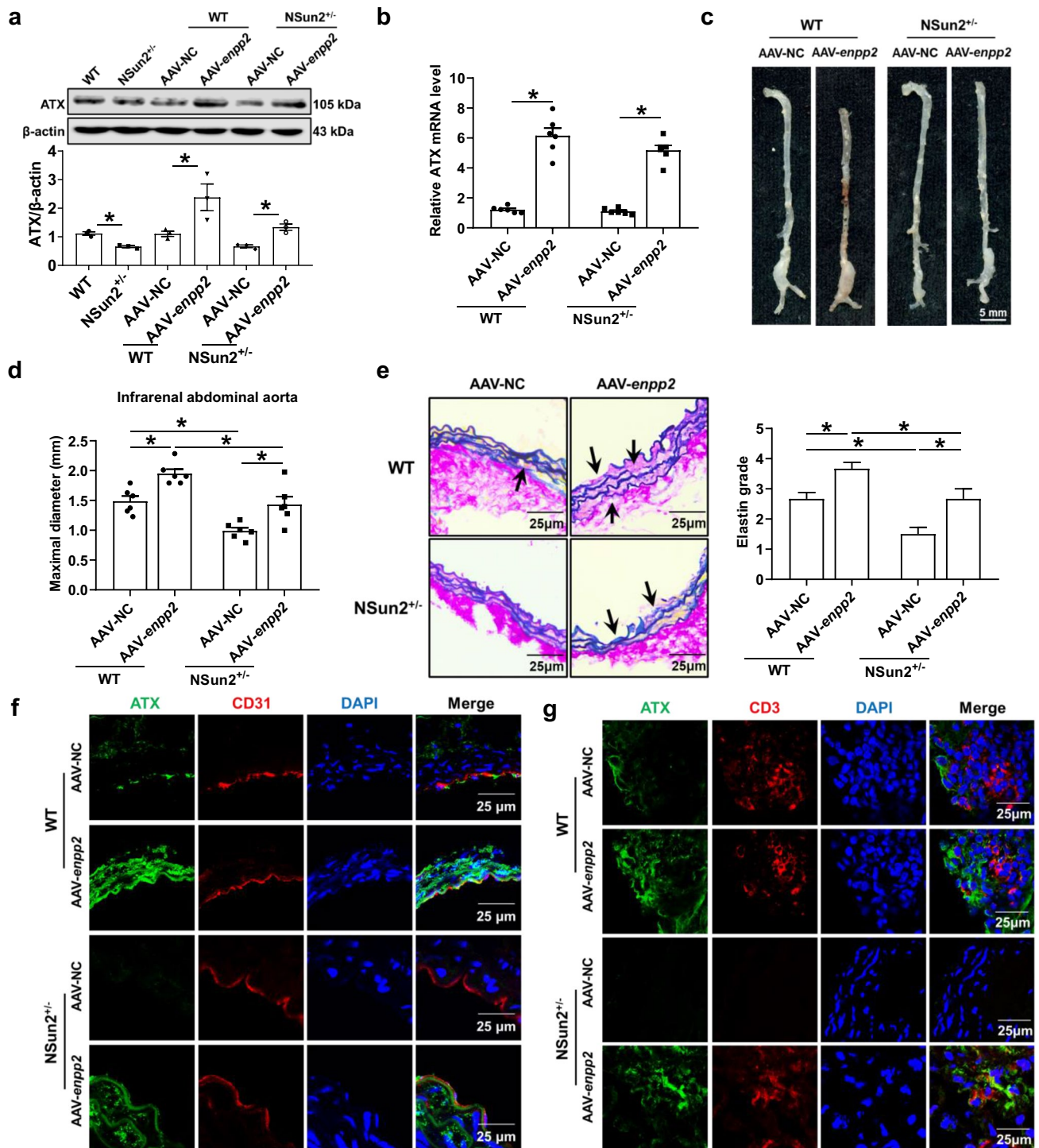


Fig. 7 Overexpression ATX in aortas aggravates AAA development in NSun2^{+/-} mice. Infrarenal abdominal aortas of 10- to 11-week-old WT and NSun2^{+/-} mice were treated with elastase to induce abdominal aortic aneurysm after the infrarenal abdominal aortas were transfected with either AAV-NC or AAV-enpp2 (10^{10} pfu) suspended in 50 μ L 30% Pluronic F-127 gel for 2 weeks. **a** Representative Western blot analysis of ATX expression in infrarenal abdominal aortas ($n=3$). **b** Real-time PCR quantification of ATX mRNA levels in infrarenal abdominal aortas ($n=6$). **c, d** Representative photographs (c) and quantification of maximal diameters (d) of infrarenal abdomi-

nal aortas ($n=6$). **e** Representative Verhoeff–Van Gieson staining and statistical analysis of elastin degradation in the infrarenal abdominal aortas ($n=6$). Scale bar, 25 μ m. **f** Representative immunofluorescent staining of ATX expression in endothelial cells (CD31 positive) in infrarenal abdominal aortas. Scale bar, 25 μ m. **g** Representative immunofluorescent staining of CD3⁺ T cells of infrarenal abdominal aortas. Scale bar, 25 μ m. Data shown are mean \pm SEM. * $P < 0.05$, by two-way ANOVA followed by Tukey's test for multiple comparisons (a, b, d, e)

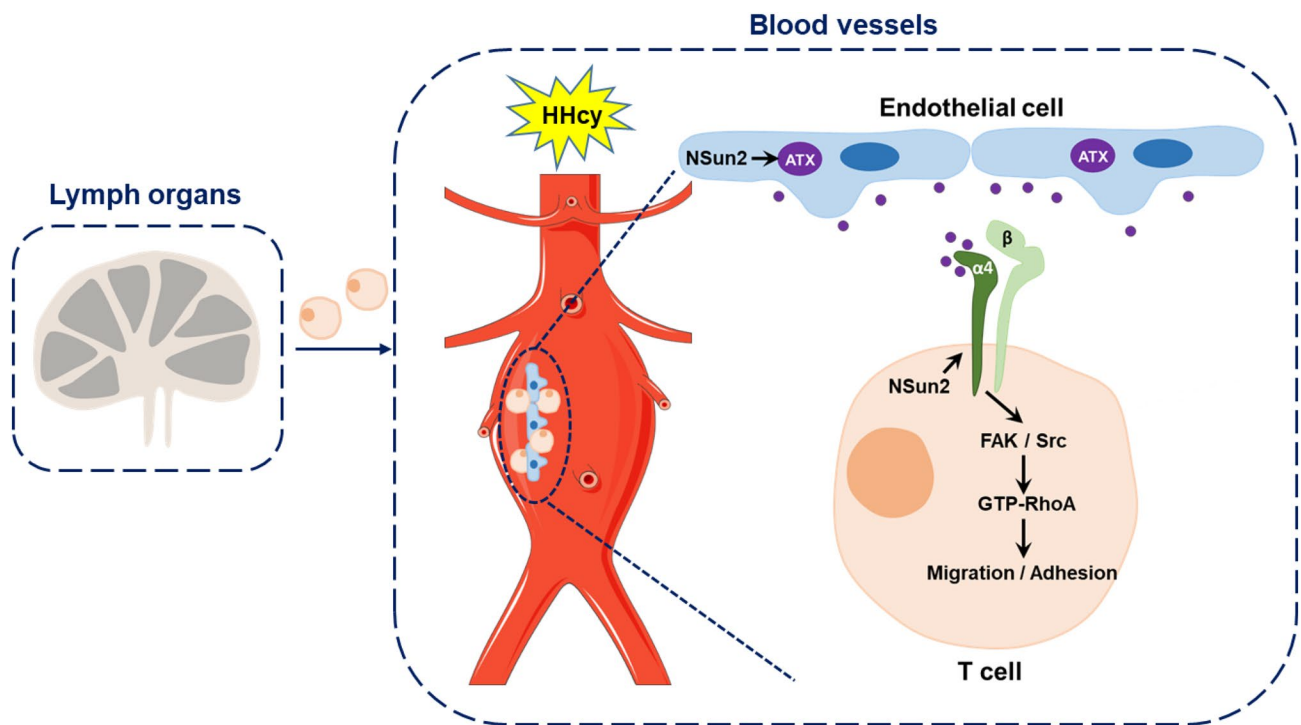


Fig. 8 Schematic representation of the proposed mechanisms. RNA methyltransferase NSun2 mediates the Hcy-promoted ATX protein expression and secretion from endothelial cells, which plays a driving role in T cell migration and adhesion to the vascular endothelium

by direct binding to integrin $\alpha 4$ and activating FAK/Src/RhoA signaling pathway in T cells and then accelerates the AAA formation and development

Discussion

The present study provided the first evidence that the RNA methyltransferase NSun2 mediates endothelial ATX protein expression and secretion and in turn promotes T cell migration and adhesion during HHcy-aggravated AAA. Mechanistically, secreted endothelial ATX directly binds to integrin $\alpha 4$ on the T cell surface and subsequently activates the downstream FAK/Src/RhoA signaling pathway (Fig. 8).

NSun2 is a tRNA and mRNA methyltransferase implicated in cell proliferation [4], stem cell differentiation [5], testis differentiation [6] and human cancers [4, 7]. In a rat model of aortic allograft arteriosclerosis, our previous study demonstrated that Hcy-induced RNA methyltransferase NSun2 upregulates ICAM-1 protein expression by methylating ICAM-1 mRNA in vascular endothelial cells, thereby increasing the adhesion of leukocytes [8]. Based on the reported study, we hypothesize that NSun2 may be more likely involved in AAA development because leukocyte migration to vessels also plays a pivotal role in AAA. As expected, the incidence of AAA and HHcy-accelerated AAA were significantly decreased in NSun2^{+/-} mice accompanied by lower attraction for T cells than it in WT mice (Figs. 1, 2). This study provides the first evidence of NSun2 regulating vascular inflammation in mice. Furthermore, RNA-seq data

showed that many genes in the PC-LPC-LPA axis, especially ATX, were upregulated in endothelial cells after Hcy treatment (Fig. 3), suggesting the involvement of cellular lipid metabolism. Subsequent *in vivo* experimental data indicated that ATX may be a new potential regulatory target for NSun2 (Fig. 4); however, the precise mechanism needs to be explored in the future. The present study was consistent with the ATX-promoted lymphocyte and tumor cell migration shown by other researchers [15, 24]. Vascular ICAM-1 is regulated by NSun2 in both rats [8] and mice. ICAM-1 expression was upregulated in the local vessel wall in AAA, which was downregulated in NSun2^{+/-} mice (Fig. S5). This result suggested that ICAM-1 may be one of the alternative explanations for changed lymphocyte accumulation in vascular lesions of NSun2^{+/-} mice, in addition to ATX.

HHcy is an independent risk factor for various cardiovascular diseases. Our series of studies have investigated several cellular and molecular mechanisms involved in HHcy-aggravated AAA formation, including the following: (a) HHcy aggravates AAA by promoting adventitial fibroblast transformation into myofibroblast by activating NADPH oxidase 4 [10]. (b) Hcy directly interacts with and activates the angiotensin II type I receptor to aggravate vascular injury and AAA formation [12]. (c) HHcy accelerates AAA development accompanied by recruitment of many more monocytes/

macrophages and T cells into the vascular adventitia and activation of macrophage NLRP3 inflammasome [10, 11]. (d) Recently, B cell-derived pathogenic anti- β 2GPI IgG and aPL antibodies were shown to contribute to HHcy-aggravated chronic vascular inflammation and AAA formation [9]. Therefore, complex effects can be induced by HHcy during AAA development. Here, RNA-seq data provided a series of new potential targets, including ATX regulated by Hcy in inflammatory endothelial cells. In vitro experiments showed that Hcy-induced ATX secretion could activate T cell chemokinesis and adhesion to endothelial cells, which deepened our understanding of Hcy-mediated vascular inflammation. Hcy induces the expression and secretion of MCP-1 and CCL5, which are chemotactic for T cells by activating CCR2 and CCR5, respectively, in human aortic endothelial cells and monocytes [32–34]. HHcy promotes the recruitment of CXCR6⁺ lymphocytes by upregulating CXCL16 and contributes to the formation and progression of atherosclerotic lesions [35]. In fact, the upregulation of several chemokines related to T cell migration, including MCP-1, CCL5, CX3CL1 and CXCL12, in elastase-treated abdominal aortas of WT mice, all of which showed a significant downregulation in elastase-treated NSun2^{+/-} mice (Fig. S6). This may also partly account for the reduction in T cell migration in NSun2^{+/-} mice. Regarding the secreted ATX to induce initiative T cell migration in circulation, ATX may likely exert earlier effects to enhance lymphocyte motility compared with other chemokines expressed by the inflammatory vessels.

A number of studies have indicated that AAA is an immunological disease accompanied by clonally expanded T cells in response to unidentified self or nonself antigens in human AAA lesions [36–38]. In the present study, we also investigated the T cell proliferation in the vascular lesions by BrdU staining in a murine AAA model. In WT AAA mice, the proliferative marker BrdU showed partial colocalization with CD3, a T cell marker, indicating the possible existence of clonally expanded T cells in the vascular lesions (Fig. S7 upper panel). HHcy dramatically increased T cell proliferation. However, this colocalization was invisible in the NSun2^{+/-} mice of the AAA group, likely because of the significant decrease in T cell number (Fig. S7 lower panels). These data suggested that NSun2 may decrease T cell recruitment and migration into the vascular lesions rather than affecting T-cell clonal expansion in situ. As reported, the identification of the T cell antigen receptor (TCR) transcripts employed by the clonally expanded T cells in AAA lesions indicates the specific antigens that elicit these T cell responses. These antigens may be responsible for the pathogenesis of AAA [39]. Therefore, it is necessary in the future to further explore whether the T cell proliferation observed in murine AAA lesions is associated with clonal expansion in situ and whether molecular mimicry plays an important

role in this process. Additionally, we found that NSun2 mediates HHcy-induced upregulation of IL-17A expression by methylating IL-17A mRNA and promoting its translation in T lymphocyte previously [40], indicating Th17 as another NSun2-regulated target. As reported, Th17 and IL-17A promoted macrophage recruitment to the vessels and contributed to AAA formation [41, 42]. Therefore, NSun2-mediated IL-17A production might also participate in AAA development. The potential effects of NSun2 on T cells per se during AAA development will be explored in the future.

T cell assistance is required for autoantibody production. Autoantibodies to aortic molecules, including anti-aortic-aneurysm-associated protein-40 (AAAP-40) IgG and anti-high density lipoprotein (HDL) IgG, have been identified in human AAA [43, 44]. In addition, we investigated the effects of elastase-induced AAA per se and AAA plus HHcy stimulation on autoantibody production in vivo and found that the level of anti-oxidized low density lipoprotein (anti-ox-LDL) antibody was increased and even higher in the HHcy group of WT mice, which was partly reversed in NSun2^{+/-} mice (Fig. S8a). With regard to anti- β 2GPI secretion, there was only a trend of upregulation in the elastase-induced AAA of the WT mice and a significant increase in the elastase + HHcy group. There was almost no influence on the HHcy-increased anti- β 2GPI secretion by NSun2 knockdown (Fig. S8b). The HHcy-related experimental data was consistent with our recent study in which B cell-derived pathogenic anti- β 2GPI IgG and aPL antibodies might contribute to HHcy-aggravated chronic vascular inflammation and murine AAA formation [9]. Actually, aPL antibody is associated with elevated levels of inflammatory markers and is an independent predictor of progressive disease in AAA patients [45, 46]. All the evidence indicates autoantibody production in AAA models; however, whether it needs T cell assistance should be determined in the future.

Endothelial cells trigger vascular remodeling by expressing adhesion molecules, which induce recruitment, migration and infiltration of inflammatory cells. The recruitment process of lymphocytes from blood circulation to the vessel wall includes cell tethering and rolling along endothelial layers, chemokine-induced cell activation, integrin-dependent cell adhesion and cell transmigration [3]. The initial tethering and rolling of lymphocytes are dependent on the interaction between selectins and their ligands. After chemokine-induced activation of lymphocytes on the endothelial layer, integrins α 4 β 1, α 4 β 7, and α L β 2 are activated to mediate firm cell arrest via binding to their ligands on endothelial cells, including vascular cell adhesion molecule 1 (VCAM-1), mucosal vascular address in cell adhesion molecule 1 (MAdCAM-1), and ICAMs [47]. The recognition and binding of active integrins and their ligands can induce integrin clustering and trigger F-actin reorganization, which further supports T cell adhesion and spreading across the

endothelium. Ren et al. [48] demonstrated that andrographolide suppressed integrin $\alpha 4$ expression and attenuated the adhesion of monocytes/macrophages to activated endothelial cells. Thus, integrin-dependent cell activation may be essential for inflammatory cell recruitment. Our results supported this fact because the integrin $\alpha 4$ neutralizing antibody anti-CD49d mAb inhibited the adhesion of T cells to HUVECs induced by ATX or Hcy (Fig. 5f). The integrin inhibitor RGDS effectively decreased the ATX-induced integrin-activated intracellular downstream FAK and Src signaling pathways (Fig. 6c), which mediated the process of cell migration as reported [49].

ATX was initially discovered as a secreted protein from A2058 melanoma cells and could enhance cell motility [50]. It obviously exists in the brain, ovary, lung, intestine, kidney and lymph nodes [24, 29]. Regarding to endothelial cells, ATX expresses in high endothelial cells of lymph nodes and in endothelial cells of zebrafish embryos [24, 51]. ATX expressed in vascular endothelial cells is known to induce tube regression [52]. In a murine AAA model, we confirmed for the first time the abundant endothelial ATX expression. The solvent-exposed surface of the N-terminal tandem SMB-like domains of ATX could bind to integrin $\alpha \text{IIb}\beta 3$ in platelet and CHO cells [53]. It has also been reported that lymphocyte integrin $\alpha 4$ and $\beta 1$ are involved in ATX-induced adhesion by using a function-blocking antibody [24]. In line with these previous reports, our results showed that integrin $\alpha 4$ did mediate the effects of ATX. More importantly, we showed the direct binding of ATX to integrin $\alpha 4$ followed by outside-in signal activation via phosphorylation of FAK and Src (Figs. 5, 6). ATX harbors various potential integrin-binding motifs, including a Leu-Asp-Val sequence for binding to $\alpha 4\beta 1$ and an Arg-Gly-Asp sequence for binding to $\beta 1$ integrins ($\alpha 5\beta 1$, $\alpha \text{V}\beta 1$, $\alpha 8\beta 1$), αV integrins ($\alpha \text{V}\beta 3$, $\alpha \text{V}\beta 5$, $\alpha \text{V}\beta 6$, $\alpha \text{V}\beta 8$) and $\alpha \text{IIb}\beta 3$ [24, 54, 55]. The exact site of ATX that binds to integrin $\alpha 4$ still requires further investigation.

Phospholipid catabolism is closely relevant to numerous vascular-associated diseases. PLD is a mediator during high phosphate-induced vascular calcification associated with chronic kidney disease [56]. HA130, an ATX lysoPLD activity inhibitor, decreases superoxide generation in pulmonary microvascular endothelial cells [57]. Our RNA-seq analysis data showed that Hcy triggered robust upregulation of PLA2 and ATX, which are phospholipases, and downregulation of lysophosphatidylcholine acyltransferase (LPCAT), a series of phospholipid synthases in the endothelium (Fig. 3a). This finding is consistent with our previous study on differentiated human adipocytes and epididymal white adipose tissue [58]. These data indicate that Hcy exerts its pro-inflammatory effects in the endothelium by affecting cellular lipid metabolism from two perspectives, including intracellular phospholipid catabolism and secreted regulatory proteins, such as ATX.

In summary, our study provides an important insight into the progress of HHcy-aggravated AAA. NSun2 mediates Hcy-induced endothelial ATX expression and secretion, thus accelerating T cell migration and adhesion to endothelium, which is a novel mechanism for aggravating vascular inflammation, matrix degradation and AAA development. NSun2 deficiency attenuates T cell recruitment and rescues HHcy-accelerated AAA development in vivo, indicating that the NSun2-ATX axis might be a potential intervention target for HHcy-accelerated vascular inflammation and AAA.

Acknowledgements This work has been funded by National Natural Science Foundation of China (81670413, 91739303, 91939105, 81770445, and 81700648). We are grateful to Professor Junjie Zhang and Dr. Xiaotian Zhang (College of Life Sciences, Beijing Normal University) for their advice and Prof. Chih-chen Wang, Dr. Lei Wang and Dr. Xun Wu (Institute of Biophysics, CAS) for the kind gift of HUVECs.

Compliance with ethical standards

Conflict of interest The authors declare that they have no conflict of interest.

References

- Weintraub NL (2009) Understanding abdominal aortic aneurysm. *N Engl J Med* 361:1114–1116. <https://doi.org/10.1056/NEJMibr0905244>
- Shimizu K, Mitchell RN, Libby P (2006) Inflammation and cellular immune responses in abdominal aortic aneurysms. *Arterioscler Thromb Vasc Biol* 26:987–994. <https://doi.org/10.1161/01.ATV.0000214999.12921.4f>
- Mitroulis I, Alexaki VI, Kourtzelis I, Ziogas A, Hajishengallis G, Chavakis T (2015) Leukocyte integrins: role in leukocyte recruitment and as therapeutic targets in inflammatory disease. *Pharmacol Ther* 147:123–135. <https://doi.org/10.1016/j.pharmthera.2014.11.008>
- Frye M, Watt FM (2006) The RNA methyltransferase Misu (NSun2) mediates Myc-induced proliferation and is upregulated in tumors. *Curr Biol* 16:971–981. <https://doi.org/10.1016/j.cub.2006.04.027>
- Blanco S, Kurowski A, Nichols J, Watt FM, Benitah SA, Frye M (2011) The RNA-methyltransferase Misu (NSun2) poises epidermal stem cells to differentiate. *PLoS Genet* 7:e1002403. <https://doi.org/10.1371/journal.pgen.1002403>
- Hussain S, Tuorto F, Menon S, Blanco S, Cox C, Flores JV, Watt S, Kudo NR, Lyko F, Frye M (2013) The mouse cytosine-5 RNA methyltransferase NSun2 is a component of the chromatoid body and required for testis differentiation. *Mol Cell Biol* 33:1561–1570. <https://doi.org/10.1128/MCB.01523-12>
- Okamoto M, Hirata S, Sato S, Koga S, Fujii M, Qi G, Ogawa I, Takata T, Shimamoto F, Tatsuka M (2012) Frequent increased gene copy number and high protein expression of tRNA (cytosine-5-)-methyltransferase (NSUN2) in human cancers. *DNA Cell Biol* 31:660–671. <https://doi.org/10.1089/dna.2011.1446>
- Luo Y, Feng J, Xu Q, Wang W, Wang X (2016) NSun2 deficiency protects endothelium from inflammation via mRNA methylation of ICAM-1. *Circ Res* 118:944–956. <https://doi.org/10.1161/CIRCRESAHA.115.307674>

9. Shao F, Miao Y, Zhang Y, Han L, Ma X, Deng J, Jiang C, Kong W, Xu Q, Feng J, Wang X (2019) B cell-derived anti-beta 2 glycoprotein I antibody contributes to hyperhomocysteinemia-aggravated abdominal aortic aneurysm. *Cardiovasc Res*. <https://doi.org/10.1093/cvr/cvz288>
10. Liu Z, Luo H, Zhang L, Huang Y, Liu B, Ma K, Feng J, Xie J, Zheng J, Hu J, Zhan S, Zhu Y, Xu Q, Kong W, Wang X (2012) Hyperhomocysteinemia exaggerates adventitial inflammation and angiotensin II-induced abdominal aortic aneurysm in mice. *Circ Res* 111:1261–1273. <https://doi.org/10.1161/CIRCRESAHA.112.270520>
11. Sun W, Pang Y, Liu Z, Sun L, Liu B, Xu M, Dong Y, Feng J, Jiang C, Kong W, Wang X (2015) Macrophage inflammatory mediates hyperhomocysteinemia-aggravated abdominal aortic aneurysm. *J Mol Cell Cardiol* 81:96–106. <https://doi.org/10.1016/j.yjmcc.2015.02.005>
12. Li T, Yu B, Liu Z, Li J, Ma M, Wang Y, Zhu M, Yin H, Wang X, Fu Y, Yu F, Wang X, Fang X, Sun J, Kong W (2018) Homocysteine directly interacts and activates the angiotensin II type I receptor to aggravate vascular injury. *Nat Commun* 9:11. <https://doi.org/10.1038/s41467-017-02401-7>
13. Magkrioti C, Galaris A, Kanellopoulou P, Stylianaki EA, Kaffe E, Aidinis V (2019) Autotaxin and chronic inflammatory diseases. *J Autoimmun* 104:102327. <https://doi.org/10.1016/j.jaut.2019.102327>
14. Zhang Y, Chen YC, Krummel MF, Rosen SD (2012) Autotaxin through lysophosphatidic acid stimulates polarization, motility, and transendothelial migration of naive T cells. *J Immunol* 189:3914–3924. <https://doi.org/10.4049/jimmunol.1201604>
15. Umez-Goto M, Kishi Y, Taira A, Hama K, Dohmae N, Takio K, Yamori T, Mills GB, Inoue K, Aoki J, Arai H (2002) Autotaxin has lysophospholipase D activity leading to tumor cell growth and motility by lysophosphatidic acid production. *J Cell Biol* 158:227–233. <https://doi.org/10.1083/jcb.200204026>
16. Shida D, Kitayama J, Yamaguchi H, Okaji Y, Tsuno NH, Watanabe T, Takuwa Y, Nagawa H (2003) Lysophosphatidic acid (LPA) enhances the metastatic potential of human colon carcinoma DLD1 cells through LPA1. *Cancer Res* 63:1706–1711
17. Yamada T, Sato K, Komachi M, Malchinkhuu E, Tobo M, Kimura T, Kuwabara A, Yanagita Y, Ikeya T, Tanahashi Y, Ogawa T, Ohwada S, Morishita Y, Ohta H, Im DS, Tamoto K, Tomura H, Okajima F (2004) Lysophosphatidic acid (LPA) in malignant ascites stimulates motility of human pancreatic cancer cells through LPA1. *J Biol Chem* 279:6595–6605. <https://doi.org/10.1074/jbc.M308133200>
18. Huang P, Xiao A, Zhou M, Zhu Z, Lin S, Zhang B (2011) Heritable gene targeting in zebrafish using customized TALENs. *Nat Biotechnol* 29:699–700. <https://doi.org/10.1038/nbt.1939>
19. Ailawadi G, Eliason JL, Roelofs KJ, Sinha I, Hannawa KK, Kaldjian EP, Lu G, Henke PK, Stanley JC, Weiss SJ, Thompson RW, Upchurch GR Jr (2004) Gender differences in experimental aortic aneurysm formation. *Arterioscler Thromb Vasc Biol* 24:2116–2122. <https://doi.org/10.1161/01.ATV.0000143386.26399.84>
20. Alsiraj Y, Thatcher SE, Charnigo R, Chen K, Blalock E, Daugherty A, Cassis LA (2017) Female mice with an XY sex chromosome complement develop severe angiotensin II-induced abdominal aortic aneurysms. *Circulation* 135:379–391. <https://doi.org/10.1161/CIRCULATIONAHA.116.023789>
21. He L, Fu Y, Deng J, Shen Y, Wang Y, Yu F, Xie N, Chen Z, Hong T, Peng X, Li Q, Zhou J, Han J, Wang Y, Xi J, Kong W (2018) Deficiency of FAM3D (family with sequence similarity 3, member D), a novel chemokine, attenuates neutrophil recruitment and ameliorates abdominal aortic aneurysm development. *Arterioscler Thromb Vasc Biol* 38:1616–1631. <https://doi.org/10.1161/ATVBAHA.118.311289>
22. Butcher MJ, Herre M, Ley K, Galkina E (2011) Flow cytometry analysis of immune cells within murine aortas. *J Vis Exp* 1:2848. <https://doi.org/10.3791/2848>
23. Gaylo-Moynihan A, Prizant H, Popovic M, Fernandes NRJ, Anderson CS, Chiou KK, Bell H, Schrock DC, Schumacher J, Capece T, Walling BL, Topham DJ, Miller J, Smrcka AV, Kim M, Hughson A, Fowell DJ (2019) Programming of distinct chemokine-dependent and -independent search strategies for Th1 and Th2 cells optimizes function at inflamed sites. *Immunity* 51(298–309):e6. <https://doi.org/10.1016/j.immuni.2019.06.026>
24. Kanda H, Newton R, Klein R, Morita Y, Gunn MD, Rosen SD (2008) Autotaxin, an ectoenzyme that produces lysophosphatidic acid, promotes the entry of lymphocytes into secondary lymphoid organs. *Nat Immunol* 9:415–423. <https://doi.org/10.1038/ni1573>
25. Fagerholm SC, Hilden TJ, Nurmi SM, Gahmberg CG (2005) Specific integrin alpha and beta chain phosphorylations regulate LFA-1 activation through affinity-dependent and -independent mechanisms. *J Cell Biol* 171:705–715. <https://doi.org/10.1083/jcb.200504016>
26. Morrison VL, MacPherson M, Savinko T, Lek HS, Prescott A, Fagerholm SC (2013) The beta2 integrin-kindlin-3 interaction is essential for T-cell homing but dispensable for T-cell activation in vivo. *Blood* 122:1428–1436. <https://doi.org/10.1182/blood-2013-02-484998>
27. Dale MA, Ruhlman MK, Baxter BT (2015) Inflammatory cell phenotypes in AAAs: their role and potential as targets for therapy. *Arterioscler Thromb Vasc Biol* 35:1746–1755. <https://doi.org/10.1161/ATVBAHA.115.305269>
28. Lu S, Deng J, Liu H, Liu B, Yang J, Miao Y, Li J, Wang N, Jiang C, Xu Q, Wang X, Feng J (2018) PKM2-dependent metabolic reprogramming in CD4(+) T cells is crucial for hyperhomocysteinemia-accelerated atherosclerosis. *J Mol Med (Berl)* 96:585–600. <https://doi.org/10.1007/s00109-018-1645-6>
29. Mills GB, Moolenaar WH (2003) The emerging role of lysophosphatidic acid in cancer. *Nat Rev Cancer* 3:582–591. <https://doi.org/10.1038/nrc1143>
30. Mitra SK, Hanson DA, Schlaepfer DD (2005) Focal adhesion kinase: in command and control of cell motility. *Nat Rev Mol Cell Biol* 6:56–68. <https://doi.org/10.1038/nrm1549>
31. Thomas SM, Brugge JS (1997) Cellular functions regulated by Src family kinases. *Annu Rev Cell Dev Biol* 13:513–609. <https://doi.org/10.1146/annurev.cellbio.13.1.513>
32. Zeng X, Dai J, Remick DG, Wang X (2003) Homocysteine mediated expression and secretion of monocyte chemoattractant protein-1 and interleukin-8 in human monocytes. *Circ Res* 93:311–320. <https://doi.org/10.1161/01.RES.0000087642.01082.E4>
33. Poddar R, Sivasubramanian N, DiBello PM, Robinson K, Jacobsen DW (2001) Homocysteine induces expression and secretion of monocyte chemoattractant protein-1 and interleukin-8 in human aortic endothelial cells: implications for vascular disease. *Circulation* 103:2717–2723. <https://doi.org/10.1161/01.cir.103.22.2717>
34. Sun W, Wang G, Zhang ZM, Zeng XK, Wang X (2005) Chemokine RANTES is upregulated in monocytes from patients with hyperhomocysteinemia. *Acta Pharmacol Sin* 26:1317–1321. <https://doi.org/10.1111/j.1745-7254.2005.00178.x>
35. Postea O, Koenen RR, Hristov M, Weber C, Ludwig A (2008) Homocysteine up-regulates vascular transmembrane chemokine CXCL16 and induces CXCR6+ lymphocyte recruitment in vitro and in vivo. *J Cell Mol Med* 12:1700–1709. <https://doi.org/10.1111/j.1582-4934.2008.00223.x>
36. Lu S, White JV, Judy RI, Merritt LL, Lin WL, Zhang X, Solomides C, Nwaneshiudu I, Gaughan J, Monos DS, Oleszak EL, Platsoucas CD (2019) Clonally expanded alpha-chain T-cell receptor (TCR) transcripts are present in aneurysmal lesions of patients with Abdominal Aortic Aneurysm (AAA). *PLoS One* 14:e0218990. <https://doi.org/10.1371/journal.pone.0218990>

37. Platsoucas CD, Lu S, Nwaneshiudu I, Solomides C, Agelan A, Ntaoula N, Purev E, Li LP, Kratsios P, Mylonas E, Jung WJ, Evans K, Roberts S, Lu Y, Layvi R, Lin WL, Zhang X, Gaughan J, Monos DS, Oleszak EL, White JV (2006) Abdominal aortic aneurysm is a specific antigen-driven T cell disease. *Ann N Y Acad Sci* 1085:224–235. <https://doi.org/10.1196/annals.1383.019>
38. Lu S, White JV, Lin WL, Zhang X, Solomides C, Evans K, Ntaoula N, Nwaneshiudu I, Gaughan J, Monos DS, Oleszak EL, Platsoucas CD (2014) Aneurysmal lesions of patients with abdominal aortic aneurysm contain clonally expanded T cells. *J Immunol* 192:4897–4912. <https://doi.org/10.4049/jimmunol.1301009>
39. Platsoucas CD, Oleszak EL (2007) Human autoimmune diseases are specific antigen-driven T-cell diseases: identification of the antigens. *Immunol Res* 38:359–372. <https://doi.org/10.1007/s12026-007-0044-9>
40. Wang N, Tang H, Wang X, Wang W, Feng J (2017) Homocysteine upregulates interleukin-17A expression via NSun2-mediated RNA methylation in T lymphocytes. *Biochem Biophys Res Commun* 493:94–99. <https://doi.org/10.1016/j.bbrc.2017.09.069>
41. Wei Z, Wang Y, Zhang K, Liao Y, Ye P, Wu J, Wang Y, Li F, Yao Y, Zhou Y, Liu J (2014) Inhibiting the Th17/IL-17A-related inflammatory responses with digoxin confers protection against experimental abdominal aortic aneurysm. *Arterioscler Thromb Vasc Biol* 34:2429–2438. <https://doi.org/10.1161/ATVBAHA.114.304435>
42. Madhur MS, Funt SA, Li L, Vinh A, Chen W, Lob HE, Iwakura Y, Blinder Y, Rahman A, Quyyumi AA, Harrison DG (2011) Role of interleukin 17 in inflammation, atherosclerosis, and vascular function in apolipoprotein e-deficient mice. *Arterioscler Thromb Vasc Biol* 31:1565–1572. <https://doi.org/10.1161/ATVBAHA.111.227629>
43. Xia S, Ozsvath K, Hirose H, Tilson MD (1996) Partial amino acid sequence of a novel 40-kDa human aortic protein, with vitronectin-like, fibrinogen-like, and calcium binding domains: aortic aneurysm-associated protein-40 (AAAP-40) [human MAGP-3, proposed]. *Biochem Biophys Res Commun* 219:36–39. <https://doi.org/10.1006/bbrc.1996.0177>
44. Rodriguez-Carrion J, Lindholt JS, Canyelles M, Martinez-Lopez D, Tondo M, Blanco-Colio LM, Michel JB, Escola-Gil JC, Suarez A, Martin-Ventura JL (2019) IgG anti-high density lipoprotein antibodies are elevated in abdominal aortic aneurysm and associated with lipid profile and clinical features. *J Clin Med* 9:67. <https://doi.org/10.3390/jcm9010067>
45. Szyper-Kravitz M, Altman A, de Carvalho JF, Bellisai F, Galeazzi M, Eshet Y, Shoenfeld Y (2008) Coexistence of the antiphospholipid syndrome and abdominal aortic aneurysm. *Isr Med Assoc J* 10:48–51
46. Duftner C, Seiler R, Dejaco C, Chemelli-Steingruber I, Schennach H, Klotz W, Rieger M, Herold M, Falkensammer J, Fraedrich G, Schirmer M (2014) Antiphospholipid antibodies predict progression of abdominal aortic aneurysms. *PLoS One* 9:e99302. <https://doi.org/10.1371/journal.pone.0099302>
47. Ley K, Laudanna C, Cybulsky MI, Nourshargh S (2007) Getting to the site of inflammation: the leukocyte adhesion cascade updated. *Nat Rev Immunol* 7:678–689. <https://doi.org/10.1038/nri2156>
48. Ren J, Liu Z, Wang Q, Giles J, Greenberg J, Sheibani N, Kent KC, Liu B (2016) Andrographolide ameliorates abdominal aortic aneurysm progression by inhibiting inflammatory cell infiltration through downregulation of cytokine and integrin expression. *J Pharmacol Exp Ther* 356:137–147. <https://doi.org/10.1124/jpet.115.227934>
49. Mitra SK, Schlaepfer DD (2006) Integrin-regulated FAK-Src signaling in normal and cancer cells. *Curr Opin Cell Biol* 18:516–523. <https://doi.org/10.1016/j.ceb.2006.08.011>
50. Stracke ML, Krutzsch HC, Unsworth EJ, Arestad A, Cioce V, Schiffmann E, Liotta LA (1992) Identification, purification, and partial sequence analysis of autotaxin, a novel motility-stimulating protein. *J Biol Chem* 267:2524–2529
51. Gibbs-Bar L, Tempelhof H, Ben-Hamo R, Ely Y, Brandis A, Hofi R, Almog G, Braun T, Feldmesser E, Efroni S, Yaniv K (2016) Autotaxin-lysophosphatidic acid axis acts downstream of apolipoprotein B lipoproteins in endothelial cells. *Arterioscler Thromb Vasc Biol* 36:2058–2067. <https://doi.org/10.1161/ATVBAHA.116.308119>
52. Im E, Motiejunaite R, Aranda J, Park EY, Federico L, Kim TI, Clair T, Stracke ML, Smyth S, Kazlauskas A (2010) Phospholipase Cgamma activation drives increased production of autotaxin in endothelial cells and lysophosphatidic acid-dependent regression. *Mol Cell Biol* 30:2401–2410. <https://doi.org/10.1128/MCB.01275-09>
53. Fulkerson Z, Wu T, Sunkara M, Kooi CV, Morris AJ, Smyth SS (2011) Binding of autotaxin to integrins localizes lysophosphatidic acid production to platelets and mammalian cells. *J Biol Chem* 286:34654–34663. <https://doi.org/10.1074/jbc.M111.276725>
54. Ruoslahti E (1996) RGD and other recognition sequences for integrins. *Annu Rev Cell Dev Biol* 12:697–715. <https://doi.org/10.1146/annurev.cellbio.12.1.697>
55. Hynes RO (2002) Integrins: bidirectional, allosteric signaling machines. *Cell* 110:673–687. [https://doi.org/10.1016/s0092-8674\(02\)00971-6](https://doi.org/10.1016/s0092-8674(02)00971-6)
56. Skafi N, Abdallah D, Soulage C, Reibel S, Vitale N, Hamade E, Faour W, Magne D, Badran B, Hussein N, Buchet R, Brizuela L, Mebarek S (2019) Phospholipase D: a new mediator during high phosphate-induced vascular calcification associated with chronic kidney disease. *J Cell Physiol* 234:4825–4839. <https://doi.org/10.1002/jcp.27281>
57. Vazquez-Medina JP, Dodia C, Weng L, Mesaros C, Blair IA, Feinstein SI, Chatterjee S, Fisher AB (2016) The phospholipase A2 activity of peroxiredoxin 6 modulates NADPH oxidase 2 activation via lysophosphatidic acid receptor signaling in the pulmonary endothelium and alveolar macrophages. *FASEB J* 30:2885–2898. <https://doi.org/10.1096/fj.201500146R>
58. Zhang SY, Dong YQ, Wang P, Zhang X, Yan Y, Sun L, Liu B, Zhang D, Zhang H, Liu H, Kong W, Hu G, Shah YM, Gonzalez FJ, Wang X, Jiang C (2018) Adipocyte-derived lysophosphatidylcholine activates adipocyte and adipose tissue macrophage Nod-like receptor protein 3 inflammasomes mediating homocysteine-induced insulin resistance. *EBioMedicine* 31:202–216. <https://doi.org/10.1016/j.ebiom.2018.04.022>

Publisher's Note Springer Nature remains neutral with regard to jurisdictional claims in published maps and institutional affiliations.